Inorganic Chemistry

Forum Article

pubs.acs.org/IC

Reducing Uncertainties Affecting the Assessment of the Long-Term Corrosion Behavior of Spent Nuclear Fuel

Thomas Fanghänel, Vincenzo V. Rondinella,* Jean-Paul Glatz, Thierry Wiss, Detlef H. Wegen, Thomas Gouder, Paul Carbol, Daniel Serrano-Purroy, and Dimitrios Papaioannou

European Commission, Joint Research Centre (JRC), Institute for Transuranium Elements (ITU), Postfach 2340, 76125 Karlsruhe, Germany

Supporting Information

ABSTRACT: Reducing the uncertainties associated with extrapolation to very long term of corrosion data obtainable from laboratory tests on a relatively young spent nuclear fuel is a formidable challenge. In a geologic repository, spent nuclear fuel may come in contact with water tens or hundreds of thousands of years after repository closure. The corrosion behavior will depend on the fuel properties and on the conditions characterizing the near field surrounding the spent fuel at the time of water contact. This paper summarizes the main conclusions drawn from multiyear experimental campaigns performed at JRC-ITU to study corrosion behavior and radionuclide release from spent light water reactor fuel. The radionuclide release from the central region of a fuel pellet is higher than that from the radial periphery, in spite of the higher burnup and the corresponding structural modifications occurring at the pellet rim during irradiation. Studies on the extent and time boundaries of the radiolytic enhancement of the spent fuel corrosion rate indicate that after tens or hundreds of thousands of years have elapsed, very small or no contribution to the enhanced corrosion rate has to be expected from α radiolysis. A beneficial effect inhibiting spent fuel corrosion due to the hydrogen overpressure generated in the near field by iron corrosion is confirmed. The results obtained so far point toward a benign picture describing spent fuel corrosion in a deep geologic repository. More work is ongoing to further reduce uncertainties and to obtain a full description of the expected corrosion behavior of spent fuel.

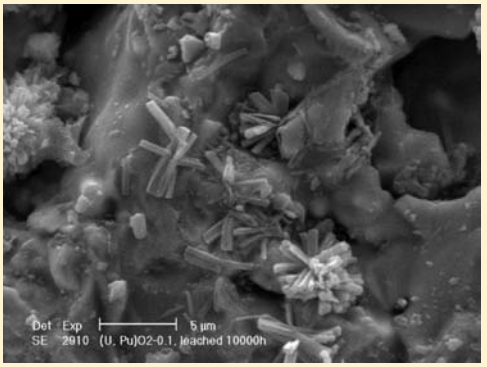

INTRODUCTION

Direct disposal of spent fuel in deep geologic repository is the option selected for the back end of the nuclear fuel cycle by many countries.[1] It is important to determine the envelope of conditions defining the safe performance of spent fuel and to assess any relevant mechanism that may cause release from the fuel and transport of radionuclides through the various barriers (natural and engineered) characterizing the near field of a repository. Most nuclear waste repositories in Europe are planned to be located at 300−500 m depth in granitic bedrock or sedimentary materials such as Opalinus, Callo-Oxfordian, or Boom clays.[2] Both granite and sedimentary materials have relatively low water permeability, although it is much lower for clay than for granitic bedrock. Typical features of these natural materials at such depths are a groundwater redox potential of −100 to −300 mV and a pH range of 7−8.5. The type and location of the nuclear waste repository determines the local groundwater composition.

Under reducing conditions, the solubility of uranium dioxide is low.[3] This is a very beneficial condition for the safety performance of the repository, considering that UO_2 is the main component of spent nuclear fuel from today's light water reactors (LWRs). All factors and processes that may alter this benign configuration deserve special attention and investigation.

Of particular importance is the determination of the fraction of the inventory of mobile (redox insensitive) fission products such as cesium and iodine, which are susceptible to prompt, or "instant", release upon the first exposure of spent fuel to groundwater. Another important factor affecting the corrosion and, in particular, the matrix dissolution behavior of spent fuel in contact with water in a geologic repository is the radiolysis of water due to the radioactive decay of radionuclides in the fuel. Although the repository is characterized by reducing conditions, the presence of some products of the radiolytic process[4−6] like H_2O_2, O_2 and radicals may cause oxidizing conditions near the fuel surface,[7] which would enhance the dissolution of uranium and other actinides. The two factors mentioned above would significantly contribute to the release of radiotoxic species from spent fuel. Both depend on the properties of the fuel as determined by its initial composition, irradiation history, and age. Specific conditions developing in the near field of the repository over long-term periods may also play an important role in determining the corrosion behavior of spent fuel. In particular, the establishment of hydrogen

Special Issue: Inorganic Chemistry Related to Nuclear Energy

Received: September 15, 2012
Published: February 22, 2013

dx.doi.org/10.1021/ic302012c | Inorg. Chem. 2013, 52, 3491−3509

overpressure conditions generated by iron corrosion in groundwater under anoxic conditions could strongly inhibit the fuel-matrix dissolution process, boosting the corrosion resistance of spent fuel against water attack. All of these processes have been and still are the subject of multiyear research programs at JRC-ITU.

Significant challenges characterize the design and implementation of effective experimental campaigns aimed at reducing the uncertainties affecting the prediction of the actual corrosion behavior of spent fuel. Because of the presence of redundant layers of corrosion-resistant containment barriers designed to isolate the nuclear waste (in this case spent fuel) from the local environment and due to the geologic stability of the repository site, it is not expected that direct contact between spent fuel and groundwater will occur in the first thousand to tens of thousands of years after emplacement. The uncertainty on the far-future time scale of the first contact (per se a positive feature of the disposal concept) sets, in turn, strong uncertainties to determine which mechanisms will govern the corrosion process. The first consideration must be to define the condition and properties of the spent fuel at the time of the first exposure to groundwater. Nuclear fission, within the boundaries of irradiation conditions and in-pile history, determines the radionuclide inventory and the physical and chemical states of spent fuel at discharge. Radioactive decay processes govern the changes occurring after discharge. The spent fuel composition, structures, and properties will evolve with time because of the cumulative effect of radioactive decay events. The evolution will determine specific parameters defining the groundwater−fuel contact scenario, such as the accessible fuel surface area and the fuel surface-to-water volume ratio (S/V), and will affect the overall physicochemical conditions to be expected in the near field at that time.[8] α-decay will be the main contributor to the accumulation of microstructural defects and helium in aging spent fuel. Moreover, α decay will generate the dominating type of radioactive emission in and around spent fuel at the time of first contact between fuel and groundwater.[9] α-Radiolysis processes would thus play the main role in determining an eventual radiolytic enhancement of the corrosion rate of the fuel.

The spent nuclear fuel available today is not fully representative of fuel aged for thousands of years or more in terms of the composition, radioactivity level, dominant type of radioactive decay and possibly also in terms of the structure and surface area. Therefore, investigation campaigns on spent fuel must be complemented by studies on analogue systems and tailored materials reproducing specific aspects expected to play a major role in the corrosion process of "old" fuel.[10,11] Moreover, analysis of the outcome of "integral" corrosion tests, including multiple parameters to mimic the complex, multicomponent near-field system is often difficult and ineffective in establishing sound cause−effect correlations. In order to understand spent nuclear fuel corrosion, elucidation of the processes on a mechanistic basis is indispensable. Thus, integral tests must be complemented by single-effect studies, which allow the derivation or validation of "simple" correlations and mechanisms.

An additional challenge affecting the experimental programs is the necessity for many experiments to reproduce in a glovebox or in a hot cell the anoxic or reducing conditions expected in most concepts of a deep geologic repository (see, e.g., refs 2 and 12). This requires the installation of complex setups including highly sensitive oxygen exclusion and monitoring systems. In many cases, it is not possible to achieve full removal of oxygen in the experimental environment: this adds a degree of uncertainty to the representativeness of the results.

Several national and international projects have been and are covering various aspects of spent fuel corrosion in a geologic repository.[13−20] The following sections will present selected highlights and the main conclusions on the processes mentioned above from published and unpublished experimental studies performed over more than 15 years at JRC-ITU. In particular, this review will present experimental results from investigations of three domains: (1) radionuclide release from different spent fuel regions representing different irradiation conditions; (2) radiolytic enhancement of fuel-matrix corrosion; (3) hydrogen-overpressure corrosion-inhibiting effects.

EXPERIMENTAL SECTION

The typical spent fuel corrosion experiment consists of exposure of a fuel specimen to a groundwater solution for a given time under controlled (as much as possible) conditions. Analyses of the leaching solution and of the sample surface after the test provide information on the radionuclide release and on corrosion mechanisms. Corrosion studies on irradiated fuel and highly radioactive materials are challenging because of limitations in handling the specimens and performing the experiments in a hot cell or a shielded glovebox. The preparation of the samples (cutting, decladding, grinding, crushing, etc.) and the handling and characterization before and after the leaching tests take place in the hot-cell (or glovebox) environment, which is prone to cross-contamination and interference from many factors (e.g., fuel fines, impurities, oxidation, etc.). In particular, a certain extent of surface oxidation is difficult to avoid during sample preparation because of the α-dose rate of the fuel and the presence of O_2 and water vapor in the hot-cell atmosphere (with typical values of 0.5 vol % and 10 ppm, respectively). Moreover, the range of conditions that can be effectively adopted and/or the spectroscopic characterization that can be applied to examine corroded surfaces is limited. A tradeoff between reproducing more closely the conditions expected in a deep geologic repository and being able to investigate a specific corrosion mechanism is often necessary. This is exemplified by the schematic illustrations of typical leaching apparatuses used in the present tests shown in Figure 1a−c and by the description of the leaching tests in the following sections (see also Annex I in the Supporting Information for more details on the experimental procedures). All leaching tests were performed at room temperature in prewashed vessels; blank tests were run to remove contributions from glass vessel leaching and from impurities in the leaching solutions.

Source-Term Experiments. A series of leaching experiments to determine the source-term data for spent fuel corrosion and radionuclide release were carried out during the last ∼15 years at JRC-ITU. All of these tests were performed in air. A detailed description of the experiments can be found in refs 21−23. Several commercial UO_2 and mixed uranium−plutonium oxide (MOX; see, e.g., refs 22 and 24) fuels from pressurized water reactors (PWRs) and boiling water reactors were used for the various campaigns: the results from leaching of two PWR fuels with average rod burnup values of 48 and 60 GWd/tHM are presented here. The nuclide inventory of the spent fuel specimens was determined experimentally by chemical analysis. Calculations using the ORIGEN-ARP code[25] were also performed as a reference to obtain the nominal inventory of a fuel pellet with the corresponding average burnup. Three types of fuel specimens were used: powder (∼0.25 g samples for the static leaching, with a typical grain size of 50−100 μm); decladded fragments (typically with a mass of 0.2−0.3 g); cladded segments of ∼1 cm length (∼9 g of fuel). Two water solutions were used for these tests: 1 mM $NaHCO_3$ + 19 mM NaCl synthetic bicarbonate (BIC) groundwater and bentonitic granitic groundwater (BGW).[21−23,26,27] A comparison between the results obtained from leaching tests using

dx.doi.org/10.1021/ic302012c | Inorg. Chem. 2013, 52, 3491−3509

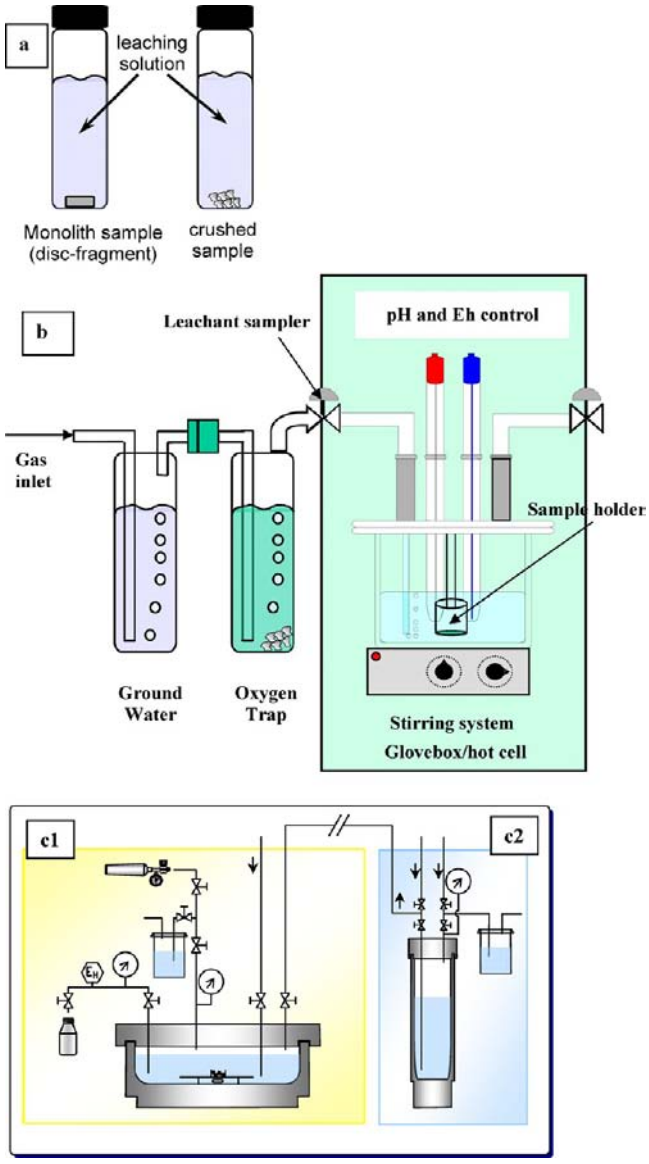

Figure 1. Schematic description of typical experimental setups for static leaching tests on irradiated fuel and materials: (a) basic leaching setup; (b) glass leaching reactors with continuous purging and pH and E_h monitoring capability of the leaching solution during the test; (c) autoclave setup used for the corrosion test on the high-burnup UO_2 fuel. The main autoclave (c1) is located in a hot cell, while the refill autoclave (c2) is located in a glovebox outside the cell. The autoclave can be refilled with fresh leachant or gas. Leachate and gas samples can be extracted for analysis.

BIC and BGW showed no difference in the observed release behavior for all of the main radionuclides. Therefore, most experiments (including those described in this paper) used BIC. The leaching experiments were performed under either static (i.e., no water flow) or dynamic conditions (using continuously stirred-tank flow-through reactors[28]). This paper describes the outcome of tests performed on fuel powder and cladded segments under static conditions with stirring in 50 mL glass tubes (Figure 1a), as representative of the whole set of experimental campaigns. The maximum time duration of these experiments was ~1 year; in general, the experiments were stopped after a steady-state radionuclide concentration level was reached in the aqueous solution. The fuel specimens were washed in acetone to remove fines before starting the leaching test. No washing in water or annealing of the spent fuel surface was done prior to the actual corrosion experiment. During the static leaching tests, the leaching solution was completely renewed after contact times of 1 and 3 days. After the second full renewal, the leachant volume in the glass tubes was kept constant (±0.1 mL) by replenishing the vessel after each aliquot sampling. The solution analysis results presented here are from nonfiltered samples (a comparison with the filtered sample is presented elsewhere[21−23]). Solution aliquots were acidified with a 1 M HNO_3 solution for high-resolution inductively coupled mass spectroscopy (HR-ICP-MS) analysis. Postleaching characterization of the corroded surfaces is performed by scanning electron microscopy (SEM).

Studies on the α-Radiolysis Effects. In order to single out the contribution of α-decay and α-radiolysis to the alteration and corrosion behavior of the spent fuel matrix, an unirradiated analogue for old spent fuel, the so-called α-doped UO_2, was used in leaching experiments. This analogue consists of unirradiated UO_2 containing different fractions of short-lived α-emitters (namely, ^{233}U and ^{238}Pu).[10,11,29−38]

Table 1 summarizes the activity and α-dose rate of sintered pellets for all α-doped UO_2 compositions. Five α-doped compositions were used, encompassing 6 orders of magnitude of specific α-activity. All batches of α-doped UO_2 were fabricated using a sol−gel technique to ensure isotropic and homogeneous distribution of the α-emissions within the UO_2 matrix. Details on the properties and activity effects of these materials are available elsewhere.[10,15,34,39,40]

Table 1. Properties of the α-Doped UO_2 Used for the Leaching Experiments

material label	added α emitter	fraction of additive (wt %)	α activity of the mixture (Bq g^{-1})	α activity at the pellet surface[a] (Bq m^{-2})	dose rate in water[a] (Gy m^{-2} s^{-1})
UO_2-10	^{238}Pu	10.0	3.8×10^{10}	2.7×10^{12}	2.8×10^{5}
UO_2-01	^{238}Pu	0.1	3.8×10^{8}	2.7×10^{10}	2.8×10^{3}
UO_2-U10	^{233}U	10.0	3.1×10^{7}	1.8×10^{9}	1.9×10^{2}
UO_2-U1	^{233}U	1.0	3.1×10^{6}	1.8×10^{8}	19
UO_2-0		0	1.1×10^{4}	8.0×10^{5}	8.3×10^{-2}

[a]The range of a ~5 MeV α-particle in UO_2 with 95% of the theoretical density is 11−14 μm (calculations using the *TRIM* code[41]). A simplistic approach is assumed here, i.e., that all α-particles emitted within 7 μm from the pellet surface reach the water. No energy loss is considered in this calculation. Grambow et al.[15] calculated a conversion factor between the specific activity and dose in a 30-μm-thick layer of water close to the surface of pellet-shaped α-doped UO_2 of $\sim 3 \times 10^{-6}$ (Gy h^{-1})/(Bq g^{-1}). See, e.g., Miller et al.[42] for a Monte Carlo analysis of the dose rate in water.

To assess the relevance of the radiolytic enhancement of fuel-matrix corrosion, it is necessary to remove the interference due to the presence of oxygen in the leaching environment. Two types of experiments were performed, under deaerated and anoxic conditions, respectively. Deaerated conditions were established by bubbling the leachant with inert gas prior to the start of the test, performed in sealed vessels (Figure 1a). Anoxic conditions were achieved by continuously purging the leachant with inert gas during the test (Figure 1b); the E_h values measured in solution at the beginning of the tests provided confirmation of the initial anoxic conditions. All tests were performed in gloveboxes with N_2 atmosphere.

This paper is focused on the results of static leaching experiments performed on disk-shaped specimens of α-doped UO_2. The results of leaching tests performed on powder samples of UO_2 containing ^{238}Pu are reported elsewhere.[29,35] Table 2 summarizes the main features of the leaching experiments described here. Deionized water (MQ) and ~1 mM carbonate water (CW) representative of a granite repository[11] were used for the leaching tests, carried out in borosilicate or Pyrex glass leaching vessels. All leachates were filtered through 450 nm membrane filters and subsequently acidified with 2 M HNO_3. Prior to the tests, the samples were annealed for 2 h at ~1300−1400 K in Ar/

dx.doi.org/10.1021/ic302012c | Inorg. Chem. 2013, 52, 3491−3509

Table 2. Main Parameters and Conditions for the Corrosion Experiments Performed on α-Doped UO_2 Reported Here[a]

experiment	α-emitter fraction (wt %)	water[b]	duration (days)	S/V (m^{-1})	condition	solution sampling
A	^{233}U 10%, 1%, 0	CW	612	1.9−2.6	deaerated	aliquot
B	^{233}U 10%, 1%, 0	CW	126	1.9−2.6	deaerated	aliquot
C	^{233}U 10%, 1%, 0	CW	365	1.9−2.6	deaerated	total renewal
D	^{233}U 10%, 1%, 0	MQ	114[d]	1.9−2.6	deaerated	total renewal
E	^{233}U 10%, 1%, 0	CW	47	0.2	anoxic	aliquot
F	^{238}Pu 10%, 1%, 0	MQ	71	∼0.5	anoxic	aliquot
G	^{238}Pu 10%, 1%, 0	MQ	46	3.9−4.1	deaerated	total renewal
H	^{233}U 1%	NaCl	80	0.07	N_2/8% H_2	EIS[c]

[a]Note that undoped UO_2 was used as the reference in almost all of the experiments. [b]CW: carbonate water. MQ; deionized water. [c]EIS: electrochemical impedance spectroscopy. [d]Extended to 334 days for the sample containing 10 wt % ^{233}U.

8% H_2 to remove damage occurring during sample preparation and to bring the UO_2 material to stoichiometry. The ratio of the sample surface to the solution volume (S/V ratio) was calculated using the geometric surface, considering both faces of the fuel disks (see Table 2). The differences in the S/V values stem mostly from differences in the water volumes used. The solutions were analyzed using HR-ICP-MS.[43,44] The error in the concentration results is estimated to be in the range 15−20%. In selected experiments, the surfaces of the fuel samples were examined by SEM after each leaching time.

Electrochemistry Experiments. Electrodes made of α-doped materials were prepared for electrochemistry tests. Slices of ∼1 mm thickness were cut from ^{233}U-doped UO_2 pellets (see Table 1). These were then cut into halves. After annealing to maintain UO_2 at stoichiometry, the half-slices were mounted upright with conductive resin on the gold-coated electrode holder. They were then impregnated under vacuum in epoxy resin (EPOTHIN). The electrodes were mechanically polished down to 1 μm diamond paste after curing of the resin. The tests were performed using a setup similar to that shown in Figure 1b. More details on the experimental procedure are provided in Annex I in the Supporting Information.

Corrosion Tests under Hydrogen Overpressure. Dedicated experimental setups have been installed in a hot cell in order to study spent fuel corrosion processes occurring under hydrogen overpressure. Achieving redox conditions close to those expected in a deep geologic repository is essential for this type of experiment. Particular care was applied in the design and installation stages to obtain a setup that could achieve and maintain truly anoxic conditions during a 5−10 year leaching experiment (Figure 1c). Moreover, the setup had to satisfy all safety guidelines and regulations to be allowed to operate under pure hydrogen overpressure inside a hot cell. The selection of materials for the inner walls of the various components of the setup (especially those in contact with the leaching solution) was a key aspect in the design stage. Steel, polymer, and glass materials were excluded because of the potential contamination and artifact generation by impurities or constituents of the compounds. A titanium autoclave was finally built for these tests. Details on the experimental procedure, and the first stages of these tests were reported by Fors et al.[45] The experiment was performed on a 260 mg sample from the radial periphery (i.e., including the high-burnup region) of a UO_2 fuel pellet from a fuel rod with 59 GWd/tHM average burnup (average sample burnup ∼67 GWd/tHM) under a hydrogen pressure decreasing from 40 to 15 bar. The leaching solution was 10 mM NaCl + 2 mM $NaHCO_3$, representing a weak saline leachant; the pH was 8.2. The initial volume of the leaching solution was 520 mL. The reported duration of the experiment was 1435 days.

Thin-Film Studies. There is a need for simplified model systems to understand basic mechanisms in complex spent fuel corrosion scenarios. A complementary approach to the study of spent fuel corrosion mechanisms is provided by using thin films deposited with relevant properties. The impact of individual components and properties on fuel corrosion is studied using model fuel surfaces, where only one given parameter is varied at a time. In such single-effect studies, the complex spent fuel system is replaced by simplified configurations, which typically consist of single-crystal or polycrystalline thin films of an actinide matrix (oxide, nitride, etc.) into which fission products are introduced by codeposition techniques. Film thickness ranges from a few atomic layers to about 1 μm. The surface composition and oxidation state are determined by photoemission spectroscopy. Morphology and elemental distribution are studied by various microscopy and spectroscopy techniques, such as SEM, transmission electron microscopy (TEM), atomic force microscopy (AFM), X-ray photoelectron spectroscopy (XPS), and X-ray diffraction (XRD). The reactivity of the surfaces is assessed by gas-exposure experiments and electrochemistry measurements.

RESULTS AND DISCUSSION

Selected results are presented addressing the conditions of the spent nuclear fuel as a consequence of reactor irradiation and its long-term alterations, the radionuclide release from different spent fuel regions representing different irradiation conditions, the radiolytic enhancement of fuel-matrix corrosion, and the effect of hydrogen overpressure in inhibiting the spent-fuel-matrix corrosion. These processes determine spent fuel dissolution and radionuclide release in the geologic repository upon contact between fuel and groundwater.

Spent Nuclear Fuel: Effects of Reactor Irradiation. The standard nuclear fuel in today's commercial reactors consists of cylindrical ceramic pellets of UO_2 or, in some cases, MOX with a diameter of ∼10 mm stacked up in metallic cladding tubes made of a zirconium alloy (zircaloy). Spent nuclear fuel is a complex, heterogeneous system, resulting from the nonuniform and nonhomogeneous accumulation of fission damage and fission products in the ceramic matrix under thermal and power gradient conditions. Strong differences in irradiation conditions (e.g., fission density, temperature) affect the different regions of a fuel pellet: the burnup (i.e., the specific energy produced by fission events occurring in the fuel, expressed here as gigawatt-day per ton of heavy metal initially present in the fuel) at the periphery of the fuel pellet is typically 2−2.5 times higher than the average pellet burnup because of fission of plutonium formed by resonance neutron capture in uranium at the outer edge of the fuel pellet; temperature gradients on the order of several hundred degrees occur from the cooler pellet periphery to the hotter center. The irradiation process induces physical and chemical alterations in the fuel: point and extended defects are formed in the crystalline lattice; the fuel swells and cracks extensively; the fission products include elements with various degrees of compatibility with the fluorite lattice of UO_2, from highly soluble lanthanides to low solubility elements precipitating as segregated oxide or metallic phases (including the so-called ε phase, a true alloy composed mainly of Mo−Ru−Tc−Pd−Rh−Te[46,47]), to essentially insoluble noble gases forming bubbles and causing swelling of the fuel. Parts a and b of Figure

dx.doi.org/10.1021/ic302012c | Inorg. Chem. 2013, 52, 3491−3509

2 show a transversal and a longitudinal section of a spent fuel rod, respectively, highlighting the typical structural features of irradiated LWR fuel.

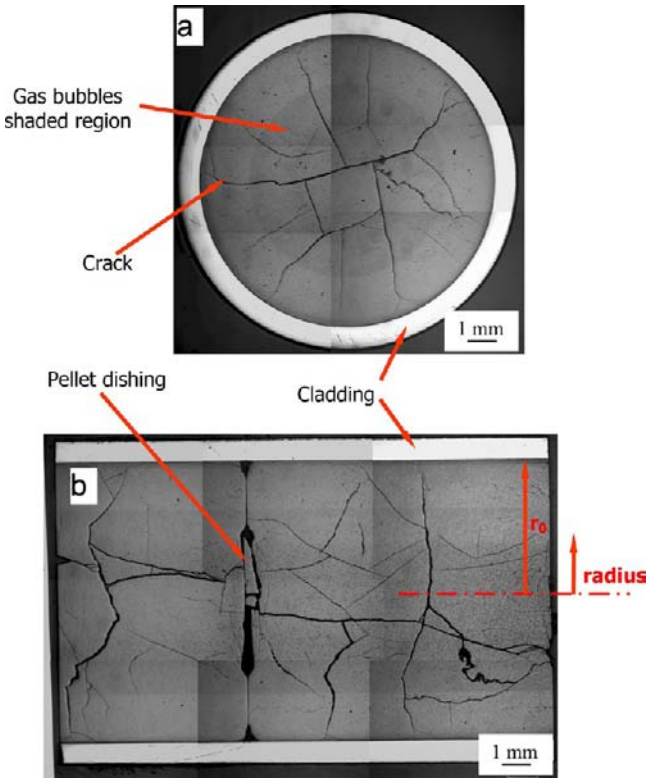

Figure 2. Typical structure of spent fuel from a LWR. Optical microscopy macrographs: (a) cross section; (b) longitudinal section of an irradiated fuel rod.

Parts a–c of Figure 3 show details obtained by optical ceramography of the fuel–cladding interface for LWR UO_2 with average pellet burnup of 20, 47, and 70 GWd/tHM, respectively. The features shown in Figure 3 are representative of the evolution of the interaction between fuel pellet and metallic cladding during irradiation in a nuclear reactor. Assuming that groundwater penetration will occur through a defect in the cladding, the interface with the cladding will be the first region of the fuel pellet to be subjected to water corrosion. At low burnup (Figure 3a), there is still a gap between fuel and cladding (similar to the fuel rod configuration at the beginning of irradiation). At higher burnup (Figure 3b,c), the gap becomes closed because of fuel swelling caused by the accumulation of fission damage and fission gas. An interaction layer is formed between fuel and zircaloy cladding, making it difficult to establish a clear boundary between metal and oxide phases. Circumferential cooling cracks formed within the fuel rather than at the fuel–cladding interface are a commonly observed feature (Figure 3c), indicating that relatively strong bonds are formed between the zircaloy cladding and the outermost regions of the fuel pellet at high burnup. Moreover, the radial periphery of the fuel pellet undergoes a significant restructuring process during irradiation; the rim or high-burnup structure (HBS) is formed. This new structure is characterized by the subdivision of the original grains (with typical sizes around 10 μm) into submicrometer grains and the relocation of the fission gas into newly formed intergranular pores (see, e.g., ref 48). The formation of this structure is already evident at 47 GWd/tHM at the rim of the fuel pellet (Figure 3b) and is fully developed in the fuel region shown on the micrograph of Figure 3c. Even at high burnup, the radial thickness of the HBS covers a small fraction of the pellet radius (on the order of tens of micrometers). Because of its location, the HBS is of high importance to determine the instant release fraction (IRF) of radionuclides and the initial stages of the fuel-matrix corrosion process in the presence of groundwater.

Solid-State Alterations in Spent Fuel after Reactor Irradiation. Nuclear fuel in the reactor operates at relatively high temperatures and undergoes significant restructuring because of irradiation effects associated mainly with the fission process; spent fuel after discharge from the reactor is maintained at lower temperatures and is subjected to radiation damage effects stemming mainly from radioactive decay events. The foremost alteration process that could cause degradation of the material properties and enhanced corrosion is associated with the buildup of α-decay damage and radiogenic helium.[8,49] It is necessary to understand mechanisms and processes responsible for the alteration of spent fuel subject to radiation damage in view of assessing its long-term mechanical and chemical conditions. Both aspects will have an impact on the corrosion behavior of the fuel in contact with groundwater: a loss of mechanical integrity of the fuel would cause an increase of the surface area exposed to water upon first contact, while possible changes of the chemical state of the fuel, in particular with respect to the oxidation state, would directly affect its dissolution behavior.

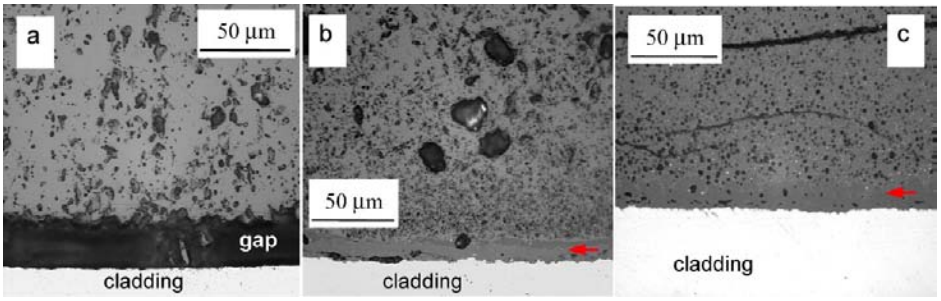

Figure 3. Optical microscopy cross-sectional micrographs showing details of the fuel pellet–cladding interface for LWR UO_2 at (a) 20, (b) 47, and (c) 70 GWd/tHM. The presence of a gap between fuel and cladding is evident in part a. At higher burnup fuel, swelling closes the gap with the cladding: the red arrows in parts b and c indicate the fuel–cladding interface layer. Typical features of the HBS (namely, a dense distribution of tiny pores) are visible in the outermost ~50 μm of fuel adjacent to the interface layer in part b and characterize the whole fuel section (>100 μm thick) shown in part c. A circumferential crack that occurred in the fuel during cooling is visible at the top of part c.

dx.doi.org/10.1021/ic302012c | Inorg. Chem. 2013, 52, 3491–3509

α-Doped UO_2 samples containing ^{238}Pu to accumulate α-decay damage and helium under accelerated conditions[50] have been extensively studied at the microstructural and macroscopic levels by TEM, SEM, optical microscopy, XPS, and XRD and their thermomechanical properties measured as a function of α-damage.[31,50−54] Figure 4 shows a TEM bright-field image of a

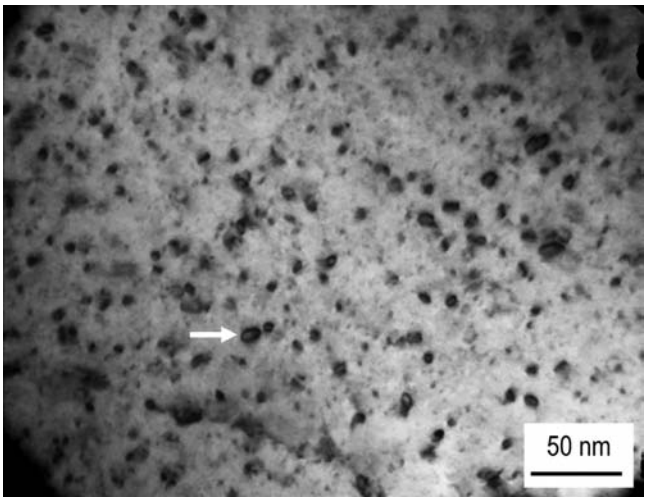

Figure 4. TEM bright-field micrograph of UO_2 containing 10 wt % ^{238}Pu having cumulated 1.2×10^{19} α-decays/g corresponding to ∼3.4 dpa. The microstructure is characterized by a large number of dislocation loops (see, e.g., the feature indicated by the white arrow).

UO_2 sample containing 10 wt % ^{238}Pu after accumulating an α-damage level corresponding to 40 GWd/tHM LWR UO_2 with a spent fuel age of $\sim 10^4$ years. The collapse of point defects causes the formation of dislocation loops and, together with the accumulation of helium-forming nanometer-sized bubbles, results in significant alteration of microscopic and macroscopic properties such as lattice swelling,[32,49] stored heat and thermal conductivity degradation,[52] hardening,[50] and the establishment of a stress field in the material.[49]

The evolution of spent fuel in a closed system, i.e., without exchange of matter, may also be affected by the potential redistribution of radionuclides by self-diffusion or α-enhanced diffusion.[55−57] To define the boundary conditions of helium diffusion, solubility measurements are performed using innovative devices both for infusion at high temperature and pressure and for the quantitative measurement of thermally desorbed helium.[53,54] These experiments so far confirmed that the solubility of helium in UO_2 is extremely low compared to the amounts generated during many decades or centuries of storage. Current work on hyperstoichiometric samples indicates that the solubility remains low also in the case of $UO_{2.08}$, showing no large effect of the oxygen-to-metal ratio on the solubility. This would support the conclusion that accumulating helium will precipitate, forming bubbles in UO_2 and causing an increase in the strain energy. Nanometer-sized helium bubbles were observed in α-doped UO_2 already at an accumulated dose of 0.5 displacements per atom (dpa) based on features resolved by TEM analysis. The excess energy associated with the accumulation of defects and helium in the lattice of UO_2 was measured using differential scanning calorimetry.[52]

Increases in the lattice parameter induced by the accumulation of gas and defects from α decay will cause swelling of the spent fuel and might, under extreme conditions, seriously degrade its mechanical integrity. α-Doped UO_2 data showed that the lattice parameter swelling saturates at values close to 0.4−0.5% at an accumulated damage level >1 dpa (∼4×10^{18} α decays/g of UO_2, corresponding in terms of spent fuel storage to >1000 years for UO_2 or ∼100 years for MOX), giving a maximum value for the lattice expansion during long-term storage.[32] Whether or not the fuel will retain the helium is important to assess its long-term mechanical stability. Thermal annealing and helium release investigations confirmed that for up to ∼2.8 dpa essentially all of the helium is retained in UO_2.[30,51,53,54] Interactions between the radiogenic helium formation and defects produced by α particles and recoil nuclei need to be understood to predict the evolution of the spent fuel rod system. Calculations by Ferry et al.[57] indicate that in spent fuel the production of helium should not result in a drastic change of the bubble pressure during the first decades of storage, mainly because of the presence of fission gas bubbles formed during reactor irradiation and other features acting as a sink for the helium.

In addition to gas accumulation and possible bubble formation, chemistry alterations linked to the radioactive decay of fuel constituents may affect the oxygen potential of the fuel. Spent fuel oxidation would result in a direct increase of the corrosion rate in contact with groundwater. The potential impact of both processes has to be considered by taking into account the heterogeneities that characterize the irradiated fuel structure. Studies at JRC-ITU are currently focused on fuel regions where the absence of a large density of preexisting gas bubbles (hence, a possible formation of overpressurized helium bubbles, causing microcracking[56−58]) and a local excess of oxygen may occur.[49]

Source Term from Leaching Tests under Oxidizing Conditions. The source term for the mobilization of radionuclides from spent fuel typically used in the performance assessment of a geologic repository consists of two components: the instant release fraction (IRF)[59] and the fraction released congruently with the matrix dissolution processes. The IRF represents the fraction of the inventory of long-lived safety-relevant and highly mobile radionuclides, such as ^{36}Cl, ^{79}Se, ^{99}Tc, ^{126}Sn, ^{129}I, and ^{135}Cs, that will be released upon first contact between fuel and groundwater, after breaching of all barriers. For interpretation of the experimental data presented hereafter, the IRF of an element at a given time is defined as the difference between the fractional release of the element in question and that of uranium. Assuming water will corrode through the cladding along a radial direction, the fuel regions likely to be accessed first by groundwater are open surfaces (cracks, crevices, etc.), the radial periphery of the fuel pellet, including the fuel−cladding gap or the interaction layer and the HBS (see Figure 3), and the grain boundaries.[14,59−63] The local inventory of the mobile radionuclides listed above at the time of groundwater contact will thus constitute the potential source term for the IRF. Given the heterogeneities characterizing the spent fuel structure and properties, and the specific effects induced by different irradiation histories and initial fuel composition (see, e.g., Figures 2 and 3), compounded by the uncertainties about the time scale of the first groundwater−fuel contact in the repository, it is difficult to define the IRF source-term parameters with a single formula valid for all cases. Most published values for the IRF are based on theoretical correlations of fission gas release data as a function of the fuel burnup and leaching data.[61,63] The experimental results on this topic are available from several

dx.doi.org/10.1021/ic302012c | Inorg. Chem. 2013, 52, 3491−3509

authors[14,59,61−73] but are relatively scarce for high-burnup UO_2 and for MOX fuels.[24,62,67,69,70,73] As a consequence of the uncertainties in defining unequivocally the IRF on the basis of universally accepted data, very conservative assumptions were made in the past for the performance assessment of a geologic repository, up to considering the whole inventory of the HBS as the IRF.[71,74,75]

To date, no experimental data are available regarding the dissolution rates uniquely of the HBS region (i.e., from samples not including also unrestructured fuel). In JRC-ITU, the release behavior of commercial high-burnup UO_2 and MOX fuels is the object of recent and ongoing experimental campaigns.[21−24,26] Particular attention is dedicated to determining the release behavior from different regions of a fuel pellet, characterized by different structures. The main objectives are to quantitatively assess the effect of the leaching solution, fuel burnup, and presence of the HBS on the IRF and on the matrix dissolution. To distinguish the IRF contributions from the gap region and the surfaces/grain boundaries immediately exposed to water and those accessed by water only after penetration along grain boundaries, an extensive program of study was undertaken using carefully prepared spent fuel samples. In particular, cladded segments containing complete cross sections of a fuel pellet and powder samples from different fuel pellet radial positions, namely, from the center (labeled CORE) and from the periphery, including the HBS (labeled OUT), were used. Because of the complexities associated with establishing reliable anoxic conditions in a hot cell for a large set of leaching tests and because of the fact that the main highly mobile species associated with the IRF (e.g., Cs) are redox insensitive, these experiments were performed in air.

A key parameter affecting the IRF and the matrix dissolution of spent fuel under oxidative conditions is the surface area available to groundwater attack. A higher matrix dissolution rate and gap IRF are measured for pellets or samples with higher specific surface area in contact with the leaching solution.[68,76,77] Ongoing experiments performed on fuel samples subjected to high power rating or ramping during irradiation confirm that fuel with a higher level of cracking, and hence higher surface area, shows a higher IRF and apparent matrix dissolution rate. Higher linear power during irradiation does not necessarily imply higher burnup. This highlights the importance of knowing the complete irradiation history of spent fuel to be able to assess its corrosion behavior.

The outcome of all of these experiments showed essentially no difference between the results for the leaching in the two groundwater solutions selected, BIC and BGW. This was attributed to the fact that both solutions contain the same amount of carbonate ion, which acts as the main complexing agent for uranium in the experimental conditions studied. In the following, only the results obtained in BIC water will be presented.

Parts a and b of Figure 5 show the concentration of uranium in the leaching solution as a function of time for powder fuel samples originating from the pellet central region (CORE) and radial periphery (OUT), respectively. The results plotted were obtained from leaching experiments using fuels with 48 and 60 GWd/tHM. The data points represent concentration values measured in leachant aliquots taken from the leaching vessel after the second total replenishment of the leaching solution, i.e., beginning after day 3 from the start of the test. The amounts released during the first 3 days of leaching are thus not included in these two plots. The horizontal dashed line on the

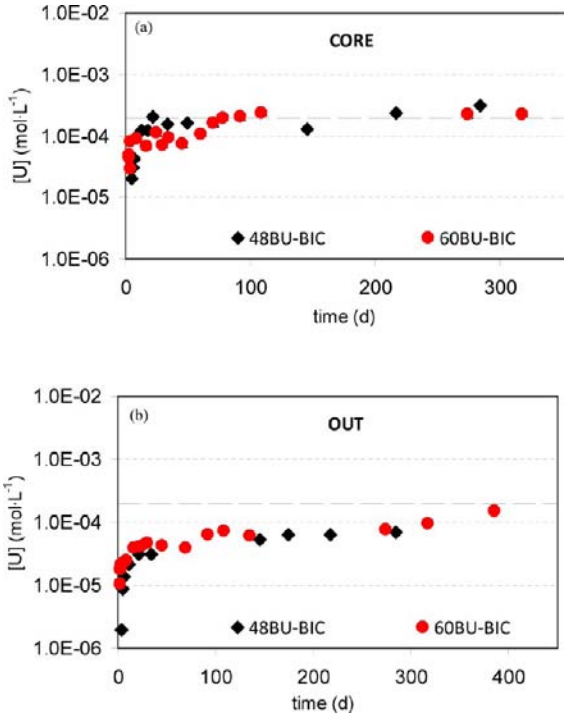

Figure 5. Uranium concentration as a function of the leaching time from static leaching experiments performed in BIC water on UO_2 fuels with 48 and 60 GWd/tHM. Powder fuel samples were leached originating (a) from the central pellet region and (b) from the pellet rim region. The horizontal dashed line represents the solubility limit for schoepite.

diagrams represents the solubility limit for schoepite $[(UO_2)_8O_2(OH)_{12}\cdot 12H_2O]$, which is the controlling solid phase under the experimental conditions adopted here and given the specific surface activity of these fuel specimens.[23] Qualitative evidence for formation of the secondary phase on the surface of the leached specimens was obtained by visual inspection. In all cases, the measured concentration values as a function of time increase until the solubility limit of schoepite is reached. The data on both diagrams reveal no difference in the dissolution behavior between the two fuels in spite of the different average burnup values. However, a difference is evident by comparing the concentration evolutions between the CORE and OUT samples. This can be explained by considering that the differences in the properties between the pellet rim and the central pellet region are significantly higher than those associated with the different average burnup values of the two fuels (see the section on irradiation effects on spent fuel). The uranium concentration values for the OUT samples are lower than the corresponding ones for the CORE specimens throughout the duration of the experiment. In the case of the samples from the central pellet region (Figure 5a), the solubility level of schoepite, at which the concentration levels off, was reached within the first 3−4 months of leaching, whereas the concentration increased more slowly for the samples from the periphery of the fuel pellets. It took more than 1 year to approach the limiting concentration level in the case of the OUT samples (Figure 5b). This highlights a trend repeatedly observed in all experiments comparing CORE and OUT: the fuel samples originating from the periphery of the fuel, which includes part of the HBS, presented lower actinide dissolution rates than the samples from the center of the pellet.

dx.doi.org/10.1021/ic302012c | Inorg. Chem. 2013, 52, 3491−3509

In order to evaluate the total amount of material released in water, including the first 3 days of leaching, and also to calculate the IRF for the relevant fission products, the experimental data were recalculated as the total fraction of inventory in the aqueous phase (FIAP) by adding the fractions released during the first 3 days of leaching to the fraction values derived from the concentrations as a function of the leaching time. Figure 6

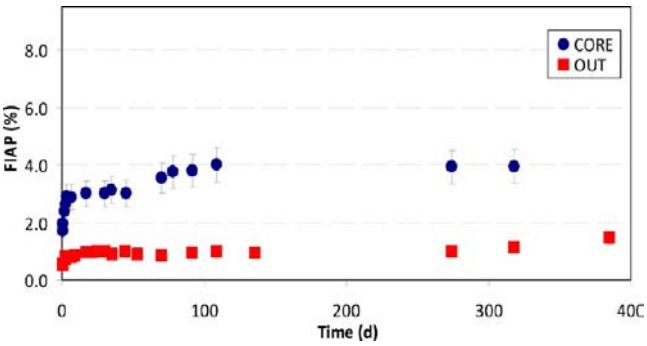

Figure 6. FIAP of uranium as a function of time from powder fuel samples from the center (CORE) and periphery (OUT) of the fuel pellet. The experiments were performed on UO_2 fuel with a burnup of 60 GWd/tHM.

shows the FIAP of uranium as a function of time for the CORE and OUT powder samples of the 60 GWd/tHM fuel. The same trends described above for the concentrations are observed when taking into account the total amount of uranium released during the leaching tests, with the CORE samples showing higher release than the OUT samples.

The small fluctuations of the FIAP and concentration data point values in Figures 5 and 6 are representative of the scatter of the concentration measurement in the leaching solution in the different aliquots collected after different contact times. This scatter does not affect the overall analysis of the trends developing during the experiment. Analysis of the FIAP plots as a function of the leaching time indicates the presence of three corrosion stages: (a) a very fast initial dissolution during the first contact time, corresponding to almost half of the total amount of uranium released during the whole leaching experiment; (b) a linear and relatively steep released fraction increase up to day 3, covering the two total replenishment cycles and accounting for approximately 25% of the total release; (c) a third stage showing an increase at a lower rate over a relatively long time span. The initial dissolution and second stage are attributed to the dissolution of the oxidized surface layer and fines present at the beginning of the experiment, while the third stage is attributed to the beginning of the fuel corrosion processes more representative of fuel behavior unaltered by sample preparation effects. The absolute magnitude of the fraction of inventory released depends strongly on the experimental configuration adopted: in the present case, the use of powdered specimens with relatively high specific surface area yields high values of the total FIAP.

Figure 7 shows the total FIAP of cesium as a function of the leaching time during approximately 4 months of leaching (the time scale used to derive the IRF) from the 60 GWd/tHM UO_2 experiments. The results for the CORE and OUT powder samples are plotted together with the data from the leaching experiment on a cladded segment of the same fuel. The release rate after the first days of leaching is higher for the CORE sample compared to the behavior of the OUT sample and of

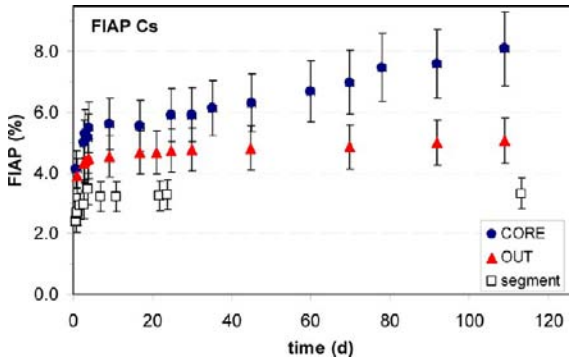

Figure 7. Fractional release of cesium from 60 GWd/tHM UO_2 as a function of time. Data for cladded segments and powder from the center (CORE) and the periphery (OUT) of the fuel pellet are shown.

the cladded segment, which showed low release after the first 3 days of leaching.

The behavior of cesium is representative of a group of elements that show consistently higher fractional release than uranium in this type of test. In all experiments and all types of fuel tested, the following trends were observed: rubidium, cesium, strontium, and molybdenum (and, in the case of static leaching, technetium) showed higher fractional release compared to uranium; these elements are thus considered as contributors to the IRF, defined here as the difference between the FIAP for a given element at a given time and the corresponding value of the FIAP for uranium; plutonium, neptunium, americium, curium, technetium (except for the static leaching), yttrium, lanthanum, and neodymium showed fractional dissolution rates similar to uranium and are considered to be released by matrix dissolution processes; finally, zirconium, rhodium, and ruthenium consistently showed lower fractional release rates compared to uranium, consistent with the fact that they are present in the fuel not only as species dissolved in the lattice but also as metallic precipitates.

There is no universally accepted definition of the contact time at which the IRF should be determined. In the present tests, by considering the amount released from CORE, OUT, and cladded segments during the first ~10 days of leaching, the IRF for cesium would be comprised in a range between 2.5% and 4.0%. This range would become slightly narrower after approximately 100 days (the time scale illustrated in Figure 7), being between 3.0% and 4.0%. Finally, the range after ~1 year of leaching would be between 3.5% and 5.5%. A more precise determination would not be significant given all the uncertainties affecting this evaluation. The ranges indicated are in line with published values[24,59,61−65,67−73,78] and represent a clear indication of the "fast" release that can be expected upon first contact between spent fuel and groundwater.

A comparison of leaching experiments performed on cladded fuel segments and powder and decladded fragments allowed one to obtain an indicative estimation of the IRF contributions due to the pellet−cladding gap and to the grain boundaries. The results of this comparison (calculated over a contact time of 10 days) confirm that the gap IRF is 1 order of magnitude higher than the grain-boundary IRF.[21,62,63] It is important to note that the particle size of the powder samples used in the leaching tests (between 50 and 100 μm) is bigger than the average grain size of the fuel.

Fission products generally showed the same trend as that observed for uranium in a comparison of the CORE and OUT

dx.doi.org/10.1021/ic302012c | Inorg. Chem. 2013, 52, 3491−3509

results. This applies not only to elements dissolving congruently with the UO_2 matrix, but also to IRF contributors. The calculated IRF values for rubidium showed no clear differences between CORE and OUT, whereas in the case of strontium, the release from the CORE sample was higher than that from the OUT sample, similar to the behavior illustrated in Figure 6. A partial and apparent exception to this important finding was obtained during calculation of the IRF for cesium in the case of the static leaching experiments presented here: although in absolute terms the fractional release of cesium was significantly higher from the CORE sample than from the OUT specimens (see Figure 7), upon subtraction of the corresponding fractions of uranium, higher values for the IRF of cesium were calculated for the OUT sample than for CORE sample. This effect may be a consequence of the low fractional release of uranium from the OUT sample (Figure 6), possibly associated with enhanced resistance against oxidation affecting the UO_2 matrix at high burnup in the presence of relatively high fractions of fission products dissolved in the lattice. Such an effect was observed for high-temperature oxidation in air[79,80] and assessed for oxidative dissolution,[81−83] although the mechanistic similarity of the two reactions is still a matter of debate.[84] Alternatively, it may be an effect associated with the radial redistribution of cesium due to the thermal gradient experienced by the fuel pellet during irradiation: such redistribution would entail a higher specific inventory of cesium at the surface of the OUT sample compared to the CORE specimen and would result in a relatively high initial release of cesium from the OUT sample.

Taking into account all of the results, it can be concluded that the fuel samples containing the HBS (OUT) showed higher resistance against water penetration and oxidative dissolution compared to the CORE samples. This has significant implications for the behavior of high-burnup spent fuel in contact with groundwater. The formation of the HBS implies that each original grain (with a size of, e.g., 10 μm) subdivides into smaller grains with a typical size of 100 nm; this corresponds to a $\sim 10^6$ subdivision factor. Moreover, the local burnup at the pellet rim is a factor of ∼2−2.5 higher than the average pellet burnup; this implies that a large fraction of the total fission product inventory is concentrated in the fuel region that will experience the first contact with groundwater. The dramatic increase in the grain-boundary area and related radionuclide inventory could be a concern upon estimation of the IRF for high-burnup fuel.[71] However, analysis of the experimental results indicates higher CORE grain-boundary dissolution rates compared to the OUT values for all of the species considered (e.g., in the case of dynamic leaching experiments by a factor of ∼4[21]). This confirms that the HBS is not an open structure, as is also indicated by the fact that during normal in-pile operation most of the fission gas inventory is retained in intergranular pores formed in the HBS.[48,85] The tightness against gas release is thus verified also against water penetration, at least within the conditions of the present oxidative corrosion experiments. An additional contribution to the stability of this structure against oxidative water dissolution at room temperature may be associated with the large amount of "stabilizing" tri- and tetravalent fission products that may buffer the oxidation of the fuel matrix.[79−81,83,84,86]

Radiolytic Enhancement of Fuel Corrosion. Once groundwater has penetrated all of the barriers protecting spent fuel in a deep geologic repository, emission of α, β, and γ radiation from the decaying radionuclides in the spent fuel will radiolyze water molecules.[5,6,87] The products of the radiolysis include oxidative ($OH^\bullet$, HO_2, and H_2O_2) and reducing (e^-_{aq}, $H^\bullet$, and H_2) species. Even though an equivalent number of oxidative and reducing species are produced, the reactivity of the molecular oxidative species is considerably higher than that of the reducing ones.[87] The effects of α[88−90] and γ[91−93] radiolysis on the dissolution of spent nuclear fuel[7,9,84,89,94−100] and, more generally, the effects of species produced by radiolysis,[101−107] have been investigated. Differences between α-, β-, and γ-radiolysis effects have also been considered.[106,108] Possible contributions to the dose rate by self-ejection of α-recoil atoms into the water have been evaluated.[31]

The assessment of the radiolysis effects on the corrosion behavior of spent fuel in a geologic repository in the remote future presents significant experimental challenges. By the time the spent fuel containers may fail, i.e., after a storage time of >1000−10000 years, the radiation field surrounding the fuel will be generated essentially by α-decays. The activity of the spent fuel available today and used for the hot-cell leaching tests is dominated by γ-decays; from this point of view, it is not representative of "old" fuel in the final repository.

In water, α particles have a range of ∼30−50 μm,[41] and the chemically highly active oxidizing species produced by radiolysis tend to react in a short time. This limits the region near the fuel surface where radiolysis effects take place to a thin film of water with a thickness of ∼40 μm. In order to obtain α-decays at the surface of the fuel, while avoiding problems related to the use of an external α-source[106] or a highly energetic α-beam,[109] α-doped UO_2 was used in leaching experiments at JRC-ITU (see Table 1). α-Doped UO_2 was used in the 1980s to study the α-radiolysis effect on the dissolution of fuel in salt brines[88] and of nuclear waste glass in salt brines and MQ[90] under oxidizing conditions. The experimental campaigns at JRC-ITU started in 1998.[10,35] Experiments on a range of α-doped UO_2 samples were conducted also at other research facilities[96,110−114] and have been included in multinational European collaborative projects, such as the Shared Cost Actions "Spent Fuel Stability" and "In-Can Processes", cofunded by the European Commission.[15,17,78,115]

Radiolysis effects are more evident under anoxic conditions, when oxidation of the fuel depends on radiolytically produced species rather than on oxygen available from the environment.[77] Therefore, the leaching experiments described here were performed under deaerated or anoxic conditions. The tests under deaerated conditions (Figure 1a) present a higher degree of uncertainty as to the exact oxygen content in the leaching vessel compared to the anoxic leaching tests (Figure 1b). However, a satisfactory convergence of the results was observed: generally, the concentrations of uranium measured in the leachates for the α-doped materials were higher than those for undoped UO_2 leached under the same conditions, with the partial exception of the α-doped samples with the lowest specific activity.

Figure 8 shows the uranium concentration in solution as a function of the leaching time for experiments A−C (Table 2) performed in CW under deaerated conditions.[11] The pH did not change significantly during all of the tests and was in the range ∼7−7.5. A clear enhanced release is observed for UO_2 with 10 wt % ^{233}U compared to the other two types of samples. The concentration values for UO_2 with 1 wt % ^{233}U are indistinguishable from those for undoped UO_2 within the time frame considered in these tests. There is good consistency among different data sets in spite of the different experiment

dx.doi.org/10.1021/ic302012c | Inorg. Chem. 2013, 52, 3491−3509

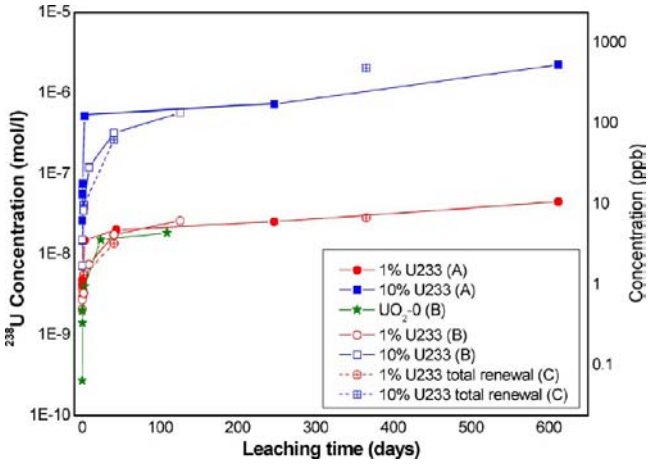

Figure 8. α-Radiolysis effect on the corrosion behavior of UO_2 doped with ^{233}U under deaerated conditions in CW shown as the uranium concentration as a function of the leaching time. Sequential leaching with aliquot sampling (experiments A and B) and with total renewal of leachant after each contact time (experiment C). A and C were carried out in the same glovebox, while B was performed in a different glovebox; in this experiment, the samples were removed from the reaction vessel and examined by SEM after each contact period.

locations and procedures adopted;[11] in particular, there is no significant difference between the data from the tests with and without replenishment. The concentration values measured for ^{233}U in solution (not shown) indicate no preferential leaching of the α-emitting isotope.

The fact that enhanced dissolution is measured in the case of UO_2 with 10 wt % ^{233}U while no significant differences are observed between the sample with 1 wt % ^{233}U and undoped UO_2 indicates that, under deaerated conditions and for the experimental time frames considered, there is a threshold to observe an α-radiolysis enhancement of UO_2 dissolution between $\sim 3 \times 10^6$ and $\sim 3 \times 10^7$ Bq/g (see Table 2). In terms of spent fuel age, this would correspond to a time range between thousands and tens of thousands of years (depending on the specific properties of spent fuel; see also Figure 12).

A comparison of the corrosion behavior of the α-doped UO_2 in CW and MQ water indicated that the release in CW is generally higher than that in MQ, as expected because of the presence of carbonate in solution. However, for the low activity and undoped UO_2, this difference was very small, and after relatively longer leaching times, the values for the total amount released converged.[11,38]

Under experimental conditions characterized by relatively high S/V ratios, the concentrations of uranium measured in solution for α-doped materials with different specific activity were indistinguishable. The values for UO_2 containing 10% ^{233}U at the end of the experiments performed under relatively high S/V (A–D; see Table 2) are similar to those measured in experiments with the ^{238}Pu-doped samples after a similar contact time (experiment G). This effect, first observed for the high-specific-activity ^{238}Pu-doped samples,[29,35] can be extended to uranium containing 10% ^{233}U, thus covering 4 orders of magnitude of α-activity (see Table 2); moreover, this effect is independent of the actual chemical composition of the α-doped material (MOX or pure uranium oxide). It must be pointed out that this consideration is not factoring in quantitatively the possible contribution from uranium reprecipitated on the vessel walls or on the sample surface. Analysis of the acid rinse solutions of the leaching vessels did not allow direct comparisons because of the different experimental procedures and setups used for the corrosion tests. The evaluation of the contributions from the rinse solution is also affected by uncertainties concerning the origin of the uranium dissolved in the acid. However, an indication of the higher release of uranium in the case of higher α-activity material was obtained.[10,37] This would imply that the mobilization of uranium from the sample surface continues throughout the contact period and produces increasing amounts of uranium reprecipitated on the vessel walls also after steady-state concentration levels were reached in solution.

The similarities in the cumulative release behavior of uranium between the ^{238}Pu-doped and 10 wt % ^{233}U-doped materials at high S/V do not correlate with the evolution of the leached surfaces. Parts a–d of Figure 9 show SEM micrographs

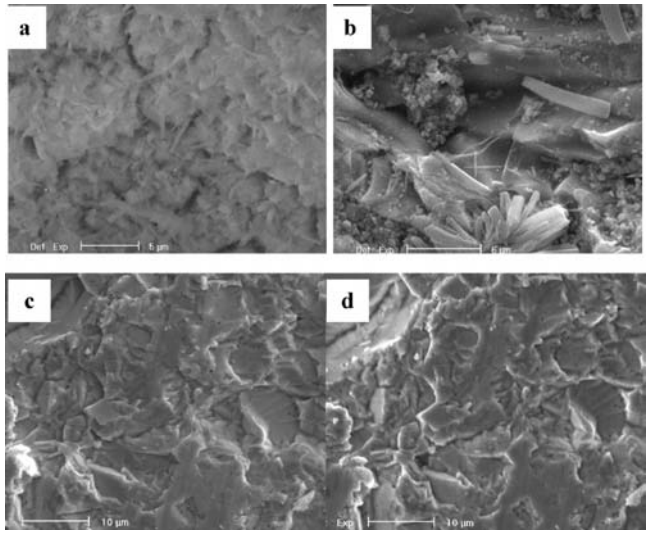

Figure 9. SEM micrographs of the surface of α-doped UO_2 disks after leaching in MQ under deaerated conditions: α-doped with (a) ~10 and (b) 0.1 wt % of ^{238}Pu leached for 284 days (from ref 38); micrographs of the same surface region of a UO_2 sample doped with 10 wt % ^{233}U after (c) 2 h and (d) 334 days of leaching (experiment D).

of α-doped UO_2 surfaces after leaching in MQ water under deaerated conditions. The micrographs on Figure 9a,b show the surface of UO_2 containing 10 and 0.1 wt % ^{238}Pu after ~284 days of leaching, respectively.[38] Significant reprecipitation, increasing with the specific α activity of the material, is evident on the surface: studtite and schoepite morphologies are visible; in the case of the highest activity material, full coverage of the surface by the higher oxide phases (mainly studtite) is observed. The SEM micrographs in Figure 9c,d show the same location on the surface of UO_2 with 10 wt % ^{233}U after (c) 2 h and (d) ~334 days of leaching in MQ. No evidence of reprecipitation processes similar to those shown for the ^{238}Pu-doped samples is observed in this case. The surface of the ^{233}U-doped sample appears essentially unchanged throughout the leaching experiments. This was also observed in the case of leaching in CW. Leaching solution analysis and XPS characterization of the surface oxidation state after leaching performed on samples with different compositions (MOX, α-doped UO_2 containing ^{233}U, etc.) and different α-activities confirmed that the extent of surface oxidation and reprecipitation of higher

dx.doi.org/10.1021/ic302012c | Inorg. Chem. 2013, 52, 3491–3509

oxides depends on the α-activity (hence, on α-radiolysis effects) rather than on chemistry effects such as the presence of plutonium in the oxide and on S/V conditions.[31,38]

A clear dependence of the concentration of uranium in solution on the activity level of the α-doped samples is observed when low S/V experimental configurations are considered (experiments E and F; see Table 2). Figure 10 shows the concentration of uranium in solution as a function of time measured under anoxic conditions (experiment E) in CW purged with Ar/0.02 vol % CO_2. The pH remained at ~7.5 during the leaching time.

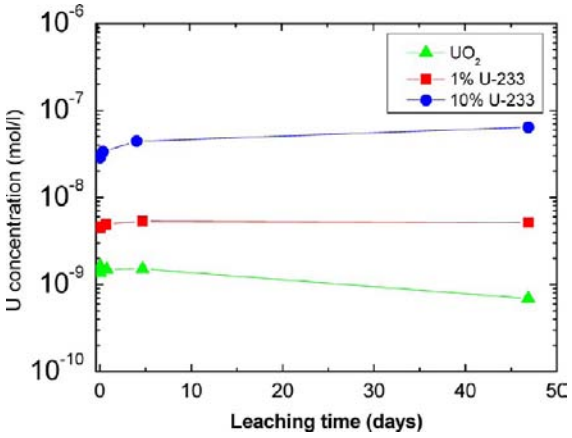

Figure 10. Concentration of uranium as a function of the leaching time in experiment E performed under anoxic conditions (Ar/0.02 vol % CO_2; see Table 2) in CW (pH 7.5).

The results for the undoped UO_2 samples show that, under anoxic conditions, corresponding to $E_h \leq 0$ in solution, no significant uranium dissolution is observed after the initial release, similar to what is seen in spent fuel leaching experiments performed under hydrogen overpressure (see the next section). In contrast with the undoped UO_2, very slow dissolution is evident from UO_2 containing 1 wt % ^{233}U, also after the initial contact times. This indicates that under anoxic conditions a small radiolytic enhancement of the UO_2 corrosion is evident also at the lowest specific α-activity level (~3×10^6 Bq/g; see Table 1). In the case of the tests under deaerated conditions, this is masked by the small amount of oxygen present in the leaching solution. In the case of UO_2 containing 10 wt % ^{233}U, the concentration of uranium in solution was almost 2 orders of magnitude higher than that for undoped UO_2. Moreover, the data provide clear evidence that additional dissolution takes place after the initial release. The different uranium concentrations in solution measured at the beginning of the leaching experiments for the three samples may be explained by a slightly higher preoxidation level of the α-doped samples. This is likely due to the reaction between the sample surface and water vapor. The sample was stored in the vessel above the water level until the E_h value of the solution had reached stable negative values. The observed differences in the initial concentration levels imply that such a preoxidation process is faster for samples with higher specific α-activity. Similar trends were observed for the results obtained under similar low S/V conditions (but in MQ water) for the ^{238}Pu-doped samples (experiment F; see Table 2[30,116]). The trends observed in experiments E and F for evolution of the concentration of uranium in solution are somewhat mirrored by the redox potential measured in the solutions. In the case of undoped UO_2 and UO_2 containing 1 wt % ^{233}U, the potential readings followed a decreasing trend as a function of time in both reaction vessels. After ~100 h, negative values of the potential are established in solution for the undoped UO_2 and, to a lesser extent, also for UO_2 containing 1 wt % ^{233}U.[116] In the case of the higher-activity α-doped materials, the E_h values remained positive and tended to increase with time. This indicates that the radiolytic production of oxidizing species can be strong enough to establish local oxidizing conditions near the fuel surface.

Various electrochemical methods were applied to investigate the aqueous corrosion of α-doped UO_2 under anoxic conditions. These have given reasonably consistent results down to 10^{-10}A/cm^2. Corrosion rates were determined by extrapolation of the current potential distribution from the anodic potential range in which the dissolution is the main process determining the free corrosion potential. Tafel extrapolation gives the corrosion current, from which the corrosion rate is calculated by Faraday's law. Under oxidizing conditions, the potential corrosion rate dependency was experimentally measured by Marx,[117] indicating a slope of 82 mV. Shoesmith and Sunder claimed values of 40−60 mV for carbonate-free solutions and a value of 90 mV for carbonate-containing electrolytes.[118,119] Using the Tafel slopes measured under N_2/8 vol % H_2 purging, corrosion rates 3 orders of magnitude lower than those measured by Marx[117] under oxidizing conditions were measured. The corrosion rates for the 10 wt % ^{233}U-doped material were about 10 times higher than those for the 1 wt % doped material, confirming the radiolytic enhancement of the corrosion rate. By purging with N_2/8 vol % H_2 instead of N_2, a significant reduction of the corrosion rate (by 1 order of magnitude or more in the 1 wt % doped material) was observed. The breakdown of the low current range was observed above 500−600 mV_{SHE}; it was explained by a rapid increase of the oxygen diffusivity (or other oxidizing agents) due to the high potential field under the experimental conditions adopted here. This represents a very extreme scenario that is unlikely to occur in a repository (see the next section). However, it demonstrates how strongly diffusion processes could affect corrosion in an underground repository

Directly after the corrosion potential measurement on 1 wt % ^{233}U-doped UO_2, potentiostatic polarization experiments were carried out on the same electrode in the same electrolyte. The potential was held for 10 h at a constant value, while evolution of the current as a function of time was measured. This was followed by electrochemical impedance spectroscopy (EIS) in the frequency range 10 kHz to 300 μHz measured during 12 h. The alternating-current amplitude was 20 mV. The applied potential was increased stepwise by +100 mV starting at 296 mV_{SHE}. EIS allowed one to determine the corrosion rates. Because of the very low corrosion rate of UO_2, especially under anoxic and reducing conditions, a very high corrosion or polarization resistance had to be measured: for instance, measurements in the range of 1−10 μHz were necessary to determine a gigaohm resistance in parallel to a capacitance of 10 μF. Considering a reasonable duration of the measurements, the practical frequency range for the measurements was at least 2 orders of magnitude higher (100 μHz to 1 mHz). The measured data had to be fit assuming a model circuit. A good fit was obtained using a simple equivalent circuit consisting of a resistance (polarization resistance) and a nonideal capacitance (double-layer capacitance) in parallel with a second resistance in series (the sum of UO_2 bulk resistance and solution

dx.doi.org/10.1021/ic302012c | Inorg. Chem. 2013, 52, 3491−3509

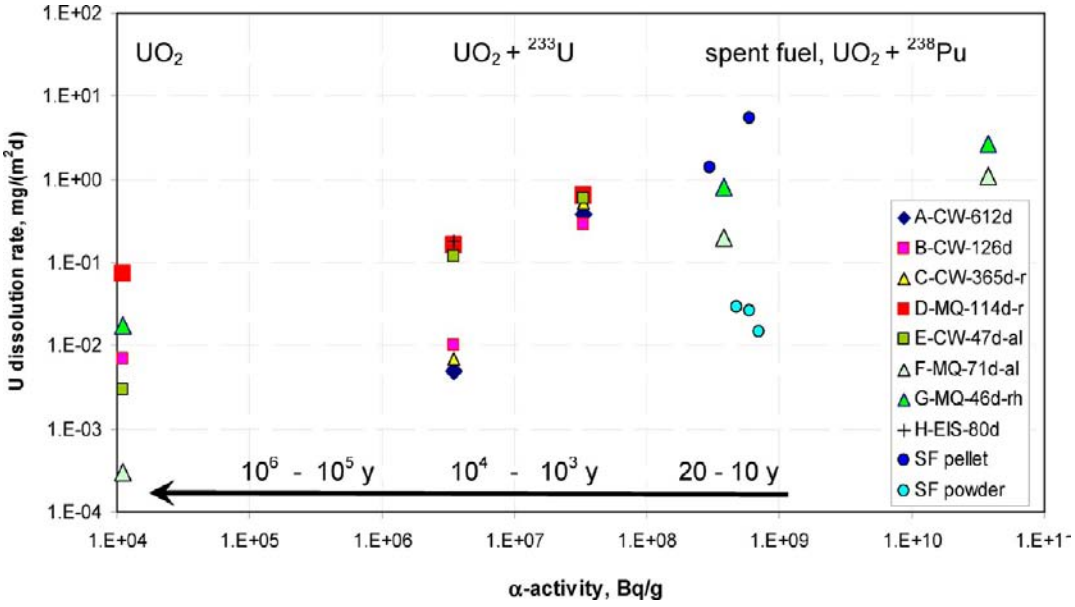

Figure 11. Dissolution rates of uranium as a function of the specific α activity obtained from all of the corrosion tests on α-doped UO_2 described here (A–H; see Table 2). Data from tests on spent fuel fragments (SF pellet) and powder samples (SF powder) are also shown. An indicative time axis is plotted at the bottom of the diagram representing the age of the LWR spent fuel corresponding to the α-activity levels investigated.

resistance). Diffusion processes, likely in a nonstirred electrolyte containing only traces of oxygen, were taken into account in the form of a Nernstian diffusion impedance in series. At the free corrosion potential, the corrosion rate can be estimated using the Stern–Geary relation $I_{corr} = B/R_{pol}$.[120,121] For UO_2 in aqueous systems, B is in the range of 20–30 mV. The corrosion rates for 10 and 1 wt % ^{233}U-doped UO_2 were calculated assuming B = 25 mV.[122] The corrosion rate for α-doped UO_2 with 1 wt % ^{233}U (experiment H) matches very well the results from leaching experiments, whereas the corrosion rate for the higher-activity sample was probably overestimated. For both samples, the corrosion rate decreased with time and with a 10-fold decrease during N_2/H_2 purging, with a slightly greater decrease for the 1 wt % doped UO_2.

Figure 11 shows the dissolution rate for uranium as a function of the specific α-activity obtained from experiments A–H (see Table 2). The specific activity levels investigated cover 7 orders of magnitude, ranging from natural unirradiated and undoped UO_2 to fresh irradiated LWR fuel with high burnup or high actinide content (MOX). The dissolution rates for spent fuel fragments and powder samples are also plotted for comparison. An indicative time scale representing the age of the spent fuel corresponding to the α-activity levels investigated is also shown. The data summarized on the diagram in Figure 11 are in good agreement with most published data and trends concerning radiolytic effects on spent fuel corrosion.[96,110−112,114,123,124]

The dissolution rates measured for undoped UO_2 show a significant scatter, covering 3 orders of magnitude. Given the very low specific activity, the dissolution behavior of UO_2 is governed by the external conditions, mainly the oxygen intrusion/presence, established in the different experimental setups and by the corresponding testing procedures. The initial dissolution of preoxidized surface layers can also have a strong impact on the overall measured dissolution rate. The influence of the external conditions affects also the values for UO_2 containing 1 wt %^{233}U, which are clustered around two dissolution rates. A first group of data points is comprised between 0.005 and 0.01 mg/(m^2 days), whereas another cluster of values range between 0.1 and 0.2 mg/(m^2 days). It is remarkable that the upper-bound dissolution rates at this specific activity were measured for the two experiments where less oxygen was present (namely, the anoxic test E and the impedance spectroscopy measurement H performed under N_2/H_2). The third experiment showing a higher corrosion rate was D, which included total renewal of the solution after each contact time. A possible explanation may be related to the low S/V condition that characterized experiments D, E, and H. However, the three experiments that showed lower corrosion rates were performed in CW and included one case with total renewal of the solution. It can be concluded that the capacity of α-doped samples to establish a radiolytically controlled dissolution regime at this activity level is relatively low and can easily be offset by perturbations of the nominal experimental conditions and/or procedure. This is evidenced by the fact that no significant difference is observed between α-doped (at this activity level) and undoped UO_2 in terms of the uranium concentration in solution for the tests under deaerated conditions. The situation is quite different when considering the dissolution behavior of UO_2 with a specific α-activity level 1 order of magnitude higher, corresponding to 10 wt % ^{233}U. The data show a remarkable convergence of the results for all five leaching experiments (A–E) to a very narrow uranium dissolution rate range, between 0.3 and 0.6 mg/(m^2 days). The strong convergence of five different experimental results clearly indicates that at this specific α-activity level under deaerated or anoxic conditions the dissolution is governed by radiolytic processes. Local oxidative conditions are established at the surface of the fuel, which control the dissolution rate.

At higher specific α-activity, corresponding to α-doped samples containing ^{238}Pu and to spent fuel, a trend toward higher dissolution rates is observed, especially at α-doping activity levels on the order of 10^{10} Bq/g. At the activity level corresponding to 0.1 wt % ^{238}Pu, which includes the results from oxidative leaching tests performed on spent fuel, significant scatter of the measured dissolution rates is observed.

dx.doi.org/10.1021/ic302012c | Inorg. Chem. 2013, 52, 3491−3509

In fact, at high specific activity levels, additional/interfering effects due to the formation of secondary phases on the fuel surface become relevant and make control of the experiment more difficult. A specific α-activity level on the order of 10^8 Bq/g is representative of spent fuel after a few years of cooling, covering the majority of spent fuel material available in a hot cell for experimental characterization. The spent fuel data plotted on the diagram illustrate the importance of possible secondary phase formation at high specific activity levels and also the impact of the surface area normalization procedure (see also the preceding section on source-term corrosion). The matrix dissolution rates derived from the leaching of fragments and powder samples differ by 2 orders of magnitude, highlighting the significance of properly defining the source-term components. All of the data points relative to undoped and α-doped UO_2 dissolution rates on Figure 11 are from leaching tests on disks and are normalized to the geometric surface. Therefore, the spent fuel data for the leaching of fragments ("SF pellet" on Figure 11) appear more consistent with the rest of the data plotted. However, the uncertainty associated with the definition of the surface area normalization term (and its evolution as a function of a progressing water attack) is still relatively high. Achieving a better understanding of the mechanisms determining the surface area available for corrosion as a function of the leaching time is necessary to further reduce the uncertainties and define the proper input for long-term corrosion predictions.

The time scale axis at the bottom of the diagram in Figure 11 is useful for evaluating the present results in the context of spent fuel corrosion in a geologic repository. On the basis of the present results, the transition (or "threshold") between a corrosion regime governed by radiolysis (hence, by spent fuel properties) and one much more dependent on external conditions is observed around a level of $\sim 3 \times 10^6$ Bq/g. This corresponds to spent LWR fuel with an age ranging between thousands and tens of thousands years. Therefore, ensuring that no contact between fuel and groundwater occurs before this time frame would essentially remove radiolysis as a major potential concern regarding the corrosion stability of the spent fuel matrix. A positive aspect to be considered is that the transition described here is derived from the outcome of experiments aiming at singling out the radiolytic enhancement of spent fuel corrosion in the absence of oxygen and excluding actively reducing agents. In fact, the overall chemistry in the near field of a deep geologic repository will be actively reducing. When actively reducing agents present in the near field (e.g., iron and/or hydrogen overpressure) are also taken into account, the experimental evidence shows that the radiolytic enhancement of spent fuel corrosion will be offset by the various inhibiting factors. In the next section, the role played by hydrogen overpressure resulting from anoxic corrosion of iron will be described and discussed.

Hydrogen Effect. All disposal concepts include technical barriers to isolate the spent fuel. For example, in the Swedish KBS-3 concept,[12] the spent fuel elements will be packaged within a waste support inner container made of cast iron inside an overpack of copper (carbon steel is also considered in other waste-packaging concepts). The low redox potential of groundwater results in a very low corrosion rate of the copper overpack, resulting in a delayed penetration of water into the inner cast-iron container.[125] Because of the absence of molecular oxygen in the groundwater, once groundwater reaches the cast-iron canister, anoxic corrosion will start. The two products of exothermic anoxic corrosion of iron in water are Fe_3O_4 (magnetite) and H_2. The chemical equilibrium pressure for this reaction is calculated to be several tens of megapascals[126] (see also refs 127 and 128). The concentration of dissolved H_2 in the solution inside the canister is expected to quickly exceed its solubility in groundwater.[129,130] Gas-phase formation occurs when the pressure of the hydrogen equals at least the hydrostatic pressure, around 5 MPa at 500 m repository depth.[35] The corresponding concentration of dissolved H_2 is approximately 40 mM.

The relatively ion-rich deep groundwaters[2] contribute to the colloid salting-out effect, thus reducing the number of colloids in these types of waters.[131,132] Two beneficial effects stem from the anoxic corrosion of iron: First, the reaction product of iron corrosion, magnetite, will react with CO_3^{2-} to form iron carbonate hydroxide, the so-called green rust $[Fe_4^{II}Fe_2^{III}(OH)_{12}CO_3]$. Green rust is known to reduce dissolved uranium(VI), in this environment mainly existing as $UO_2(CO_3)_3^{4-}$, to the much less soluble amorphous uranium-(IV) dioxide.[133,134] Additionally, the mobility of plutonium and americium decreases significantly because of their sorption onto the iron corrosion products.[135,136] Second, the presence of dissolved H_2 in contact with spent nuclear fuel will significantly reduce its corrosion rate in comparison with the corrosion of UO_2 under an Ar atmosphere.[135−139]

Several campaigns of experimental studies have been performed at JRC-ITU on the spent fuel−H_2O−H_2 system expected inside the corroded canister in a deep geologic repository. The results confirm that after an initial congruent oxidative dissolution of the fuel, which fades away within ~1 day and is followed by reduction and reprecipitation of the dissolved uranium, a regime is established characterized by a very low concentration of uranium in solution,[45,140] close to the thermodynamic solubility of uranium(IV) in water.[3]

Figure 12 shows the concentration of H_2, cesium, uranium, and plutonium measured in the leaching solution as a function

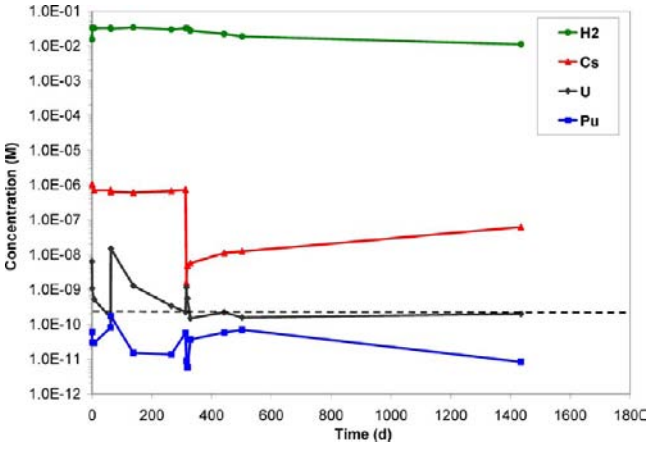

Figure 12. Concentration of dissolved H_2, cesium, uranium, and plutonium in the leaching solution in contact with spent nuclear fuel as a function of time. The concentration was measured at discrete times (represented by the symbols on the diagram). The experiment lasted 1435 days. The concentration spikes after 63 and 313 days of leaching are due to oxygen intrusion caused by leachant refill and total leachant renewal, respectively. The dotted line represents the steady-state uranium concentration of 2×10^{-10} M, which is the "baseline" concentration, which characterized this corrosion experiment in the absence of external perturbations.

dx.doi.org/10.1021/ic302012c | Inorg. Chem. 2013, 52, 3491−3509

of time during the spent fuel corrosion experiment performed using the leaching apparatus illustrated in Figure 1c. The concentration values at the beginning of the experiment are consistent with the fast dissolution of an oxidized layer present on the fuel surface (as mentioned in the Experimental Section). This initial dissolution burst is rapidly offset for the redox-sensitive uranium under the strong reducing conditions of the leaching environment. The concentration values of uranium decreased very rapidly, within a few hours after the beginning of the test reaching a steady-state value of $\sim 2 \times 10^{-10}$ M. This low uranium concentration is close to the thermodynamic solubility of uranium(IV) in water[3] and similar to results from spent fuel corrosion tests reported by Spahiu et al.[138,141] In the absence of external perturbations of the system, this concentration level was measured despite a constant α dose rate in water of ~0.5 Gy/s, yielding a continuous production of oxidative species, such as H_2O_2, at a rate of $\sim 1 \times 10^{-8}$ M/day. However, no H_2O_2 could be measured in the leachate after a corrosion time of 313 days (the detection limit was 1×10^{-6} M).

Two discontinuities are noticeable on the diagram in Figure 12: the concentration changes after 63 and 313 days of leaching were caused by air (oxygen) intrusion during a leachant refill and the leachate total replenishment, respectively. Mass spectrometric analysis of the atmosphere inside the autoclave after 313 days of corrosion determined a nitrogen concentration of 1650 ppm; this would imply that 2.3×10^{-4} mol of O_2 had entered the autoclave. However, the oxygen concentration was below the detection limit of 10 ppm, indicating very fast consumption. In fact, despite the intrusion of oxygen into the autoclave on days 63 and 313, the concentration of uranium returned to a low level of $\sim 2 \times 10^{-10}$ M, which was maintained for the remaining duration of the experiment. The decreasing uranium concentration after the spikes associated with the oxygen intrusion events was caused by reduction and reprecipitation of the initially dissolved uranium. The oxidation/reduction reactions affecting uranium in this environment made its concentration in the leaching solution as a function of time an unreliable indicator for fuel-matrix dissolution.

Under the present conditions, high-solubility, redox-insensitive cesium (namely, ^{137}Cs) could be used more effectively as an indicator for overall spent fuel corrosion; an increase in the cesium concentration indicated dissolution of the fuel matrix or newly opened grain boundaries. The profile of the cesium concentration as a function of time, shown in Figure 12, shows clear evidence of the initial dissolution "burst" caused by dissolution of an oxidized surface layer from the fuel. The total released fraction of inventory of cesium during the first hours of leaching was ~3.5%. This value is well in line with the IRF data obtained from the source-term experiments described above. After the initial release, no more cesium appeared to be dissolving. In fact, the relatively high concentration level reached during the initial release (however, still 1 order of magnitude lower than the level measured in the oxidative source-term experiments described in this paper) was masking any further release from the fuel. This was confirmed by the fact that, unlike uranium and plutonium, the cesium concentration level was unaffected by the oxygen intrusion after 63 days of leaching. A total leachate exchange on day 313 was performed with the aim of removing the cesium dissolved at the beginning of the experiment, in order to follow more clearly the cesium concentration changes and thus the fuel corrosion process. In fact, the concentration evolution of cesium after day 313 showed a relatively rapid initial increase, corresponding to the uranium and plutonium concentration increases associated with the consumption of the oxygen that had entered the autoclave, followed by a slower increase over approximately 90 days to $\sim 1 \times 10^{-8}$ M; thereafter, the concentration increased at a much slower rate, reaching a level of $\sim 6 \times 10^{-8}$ M after ~1000 days of further leaching. These concentration levels are 3 orders of magnitude lower than the values measured in leaching tests under oxidizing conditions and are indicative of an extremely slow fuel corrosion process.

Generally, the plutonium concentration changes followed those of uranium; however, a more variable tendency of the concentration profile as a function of time was evident, especially during time intervals when the uranium concentration was stable at the minimum of $\sim 2 \times 10^{-10}$ M. A possible explanation for the fluctuations of the plutonium concentration could be associated with a reduction of the less soluble plutonium(IV) to the more soluble plutonium(III).[142]

The redox potential was measured during the first ~500 days of the experiment. The trends observed correlate well with the operations of the autoclave. Each autoclave operation involving the opening of a connection valve, for example, during the rinse action, corresponded to an increase of the redox potential (in any case, all detected air intrusion events never caused the E_h value to exceed -100 mV_{SHE}); thereafter, the potential rapidly decreased to the steady-state level. The rapid decrease of E_h confirms the fast consumption of intruded O_2, in addition to radiolytic oxidizing species. Between the air intrusion events, the redox potential was stable within a range of -375 to -450 mV (steady state). The redox monitoring proved to be a very sensitive tool to detect any perturbation in the system.

The same behavior as that described here was observed in corrosion experiments performed in an autoclave under hydrogen overpressure in 10 mM NaCl + 2 mM HCO_3^- solutions, at pH 7–9, using spent MOX fuel over a contact time period of 4 years[140] and also on α-doped UO_2 containing 10 wt % ^{233}U.[143] In these cases, the final uranium concentration was as low as 10^{-10}–10^{-11} M.[143] In addition to the low steady-state concentration values, the experiments on α-doped UO_2[34,143] allowed the direct spectroscopic analysis of the leached UO_2 surface. XPS of the 10 wt % ^{233}U-doped UO_2 surface after 2.2 years of leaching confirmed that the sample surface was stoichiometric UO_2.

In the present experiment on high-burnup UO_2, a decrease of the hydrogen overpressure from 40 to 15 bar was implemented: no effect of the decreasing concentration of dissolved H_2 on the concentration values of cesium, uranium, and plutonium was detected. The tests on MOX fuel, however, showed that immediately after switching from H_2 to a pure Ar atmosphere the spent fuel started to congruently dissolve at a relatively fast rate.[140] Therefore, it can be concluded that H_2 is an essential part of the uranium reduction reaction. Spent fuel corrosion experiments indicate that the uranium reduction reaction between the dissolved H_2 and the spent fuel surface stops playing a significant role only at dissolved H_2 concentrations of $\leq$1 mM;[140] calculations show that concentrations as low as 0.1 mM would inhibit the complete dissolution of spent fuel aged 100 years or more.[144]

On the basis of the experimental data produced so far, the boundary conditions (prerequirement) for the system spent fuel–H_2O–H_2 to keep the balance between the oxidative dissolution due to α-radiolysis and the reduction reaction involving H_2 on the spent fuel surface, and hence the beneficial

dx.doi.org/10.1021/ic302012c | Inorg. Chem. 2013, 52, 3491–3509

effect of reducing spent fuel corrosion, are (i) a fuel or fuel surface close to stoichiometry (O/U < 2.01), (ii) a carbonate concentration in solution of $\geq 10^{-3}$ M, pH range 7−9, (iii) dissolved $[O_2] < 1 \times 10^{-8}$ M, and (iv) dissolved $[H_2] > 1 \times 10^{-3}$ M. All of these conditions are expected to occur in a deep geologic repository.

The present experiment confirmed a uranium concentration level in water of 2×10^{-10} M in the presence of spent fuel fragments and H_2, clearly indicating the presence of a uranium(IV) phase. While the mechanisms governing the oxidative dissolution of spent nuclear fuel are known[81,86,145,146] (see also the review by Eriksen et al.[84]), the mechanisms responsible for the reduction of uranium in the system spent fuel−H_2O−H_2 are still not fully understood. A number of possible explanations were proposed in the literature for the observed low uranium concentration measured during corrosion of spent fuel in the presence of H_2, related to (i) the homogeneous reaction between H_2 and radiolytic oxidants, (ii) surface-catalyzed decomposition of H_2O_2 on metal oxide surfaces, (iii) catalytic dissociation of H_2 on metallic fission product precipitates (the so-called ε phase), (iv) the reaction of Fe^{2+} with radiolytic oxidants, and (v) catalytic dissociation of H_2 on UO_2. Of particular relevance is the role played by the Fe^0 and Fe^{2+} phases in reducing uranium and other redox-sensitive dissolved elements. Relevant findings and the proposed mechanisms are discussed in Annex II in the Supporting Information.

CONCLUSIONS

Several campaigns of experimental studies are performed at JRC-ITU with the aim of reducing the uncertainties affecting the prediction of the spent fuel corrosion behavior in contact with groundwater in a deep geologic repository. Experiments on spent fuel and multicomponent tests are complemented by single-effect studies using model materials. Because the time scale of the first fuel−water contact is not known and given the trends affecting the burnup and irradiation history for spent fuel from LWR reactors, a broad range of parameters covering a broad scale of conditions and properties may be relevant to determine the long-term behavior of spent fuel. The aim, whenever possible, is to identify key mechanisms and processes to be able to develop a consistent understanding of relevant phenomena.

The main objective of ongoing and future research activities is to develop suitable predictive tools to determine relevant fuel properties, to define the IRF of radionuclides, and to identify key factors governing the corrosion behavior of the UO_2 matrix starting at the time of the first spent fuel−groundwater contact.

The proper definition of the surface area of spent fuel is extremely important to evaluate the long-term corrosion behavior. An important role in determining the surface properties of the fuel is played by the irradiation history: leaching results show that power excursions or other anomalous events causing cracking and thermal redistribution of mobile fission products have a strong impact on the corrosion behavior in water, possibly even stronger than the actual burnup of the fuel. Lattice swelling of α-doped UO_2 subjected to the accelerated accumulation of α-decay damage and helium up to a damage level of a few displacements per atom, corresponding to spent fuel after thousands of years of storage, shows saturation at 0.4−0.5%.[32] The relevance of micro-cracking processes induced by nanometer-sized helium bubbles in spent fuel[56] is to be further investigated. Extensive cracking of spent fuel would dramatically increase the surface available for water attack in the repository.

Static leaching tests on spent fuel fragments and powder samples from different fuel pellet regions confirm that the highest IRF values, measured for cesium, are on the order of a few percent of the local inventory. The corrosion rates for fuel samples from the radial periphery of a fuel pellet are lower than those for samples originating from the central pellet region. This is important because the rim of the pellet likely will be the first region of the fuel in contact with groundwater. This region experiences significantly higher burnup during irradiation; hence, it contains a higher concentration of fission products and actinides. The present results indicate that the formation of the HBS, characterized by a much higher specific grain-boundary surface, does not cause enhanced radionuclide release. On the contrary, its tightness (and possibly the oxidation buffering power due to the high local concentration of some fission products) provides higher resistance against groundwater corrosion. On the basis of the present findings, the adoption of ultraconservative IRF values for the release from this region appears unjustified.

The extent and boundaries of the radiolytic enhancement of fuel-matrix corrosion due to α-radiolysis were investigated using α-doped UO_2 to reproduce specific activity levels corresponding to spent fuel with an age up to $>10^4$ years. The results obtained show a transition occurring at a specific activity level around $\sim 3 \times 10^6$ Bq/g from a radiolysis-controlled regime to a solubility-controlled regime where radiolysis is not the dominating factor determining fuel corrosion rates. The simultaneous influence of additional parameters, such as the specific area exposed to groundwater, the S/V ratio, and the formation of secondary phases on the fuel surface, has to be further assessed.

The extension of the experiments to more realistic (and complex) scenarios involving spent fuel in a deep geologic repository requires one, in the case of the radiolytic effect, to move from anoxic to reducing conditions. The results from a series of experiments performed on the spent fuel−H_2O−H_2 system to investigate the effect of hydrogen overpressure expected inside the corroded canister in a deep geologic repository confirm that a steady-state regime is established characterized by very low concentration of uranium in solution,[45,140] close to the thermodynamic solubility of uranium(IV) in water.[3] The hydrogen-overpressure effect can counterbalance the oxidative conditions present at the fuel surface due to α radiolysis and therefore hinder/stop the dissolution of the spent fuel and thereby the release of long-lived fission products. Most experiments performed so far have been focused on the confirmation of the hydrogen effect and did not include the simultaneous effects by multiple agents present in the near-field system. For instance, reactions that interact with the produced hydrogen radicals may interfere with or even stop the hydrogen-induced reduction of uranium. On the other hand, other species, for instance iron, will play a similar role as hydrogen, contributing to inhibit spent-fuel-matrix oxidation and dissolution. The objective of ongoing and future investigation programs is to gradually bring together the key mechanisms active in such a complex system due to the combined effect of all relevant species controlling the actual near-field conditions.

dx.doi.org/10.1021/ic302012c | Inorg. Chem. 2013, 52, 3491−3509

■ ASSOCIATED CONTENT

Supporting Information

Details on the experimental procedures for the leaching tests (Annex I) and proposed mechanisms for the hydrogen-overpressure corrosion-suppressing effect and tailored material studies (Annex II). This material is available free of charge via the Internet at http://pubs.acs.org.

■ AUTHOR INFORMATION

Corresponding Author

*E-mail: vincenzo.rondinella@ec.europa.eu. Tel. +49 7247 951279.

Notes

The authors declare no competing financial interest.

■ ACKNOWLEDGMENTS

Most experimental campaigns referred to in this paper have been or are performed within the frame of bilateral collaboration or international projects. In particular, the oxidative source-term studies are to a large extent performed in the frame of collaboration with ENRESA, UPC, and CTM (Spain). The studies on the hydrogen effect and the repository conditions are the subject of collaboration with SKB (Sweden). A significant amount of α-radiolysis studies in the 1990s were the object of collaboration with CIEMAT (Spain). Many experiments were performed and have received funding in the frame of the European Commission (DG-RTD) cofunded projects: "Spent Fuel Stability" (FP5/1998-2002 under grant agreement no. FIKW-CT-2001-00192), NF-PRO (FP6/2002-2006 under grant agreement no. FI6W-CT-2003-02389), ReCosy (FP7/2007-2013 under grant agreement no. 212287), and FIRST-Nuclides (FP7/2007-2013 under grant agreement no. 295722). Many colleagues of partner organizations (KIT, CEA, SCK-CEN, Nagra, NNL, DoE, and NRC) have contributed to various extents and/or are part of the networks in which some of the R&D projects are embedded. Special acknowledgements must go to the suppliers of the spent nuclear fuel used for the leaching experiments, namely, to AREVA NP. Last but not least, many ITU colleagues, visiting scientists, Ph.D. students, and Postdoc fellows have provided invaluable contributions during the last 2 decades. Among others are the following: J. Cobos-Sabate for the radiolysis studies, E. Gonzalez-Robles and F. Clarens for the oxidative source term, P. Fors for the hydrogen effect, and V. Wasselin-Trupin, C.G. Alecu, and A. Seibert for the electrochemistry studies.

■ REFERENCES

(1) EC 2011, COUNCIL DIRECTIVE 2011/70/EURATOM of July 19, 2011, establishing a Community framework for the responsible and safe management of spent fuel and radioactive waste. Official Journal of the European Union, L199/48, Feb 8, 2011.

(2) Carbol, P.; Wegen, D. H.; Wiss, T.; Fors, P. Spent Fuel as Waste Material. In *Comprehensive Nuclear Materials*; Konings, R. J. M., Ed.; Elsevier: Amsterdam, The Netherlands, 2012; Vol. *5*, pp 389−420.

(3) Parks, G. A.; Pohl, D. C. *Geochim. Cosmochim. Acta* **1988**, *52* (4), 863−875.

(4) Allen, A. O.; Hochanadel, C. J.; Ghormley, J. A.; Davis, T. W. *J. Phys. Chem.* **1956**, *56*, 575.

(5) Allen, A. O. *The Radiation Chemistry of Water and Aqueous Solutions*; D. Van Nostrand Co. Inc.: Princeton, NJ, 1961.

(6) Allen, A. O. *Actions Chimiques et Biologiques des Radiations*, 5th ed.; Academic Press: London, 1961; p 1.

(7) Grambow, B.; Werme, L. O.; Forsyth, R. S.; Bruno, J. *Mater. Res. Soc. Symp. Proc.* **1990**, *176*, 465−474.

(8) Rondinella, V. V. Failure mechanisms of high level nuclear waste forms in storage and geological disposal conditions. In *Handbook of advanced radioactive waste conditioning technologies*; Ojovan, M. I., Ed.; Woodhead Publishing: Cambridge, U.K., 2011; Chapter 13, pp 397−432.

(9) Sunder, S. *Nucl. Technol.* **1998**, *122*, 211−221.

(10) Rondinella, V. V.; Matzke, Hj.; Cobos, J.; Wiss, T. *Mater. Res. Soc. Symp. Proc.* **1999**, *556*, 447−454.

(11) Rondinella, V. V.; Cobos, J.; Wiss, T. *Mater. Res. Soc. Symp. Proc.* **2004**, *824*, 167−173.

(12) SKB 1983. *Final storage of spent nuclear fuel—KBS-3*; Swedish Nuclear Fuel Supply Co./Division KBS: Stockholm, Sweden, 1983.

(13) Johnson, L. H.; Poinssot, C.; Ferry, C.; Lovera, P.; Poulesquen, A.; Miserque, F.; Corbel, C.; Cavedon, J. M.; Adriambololona, Z.; Wegen, D.; Carbol, P.; Glatz, J. P.; Cobos-Sabate, J.; Serrano, D.; Rondinella, V. V.; Wiss, T.; Grambow, B.; Spahiu, K.; Kelm, M.; Metz, V.; Loida, A.; Kienzler, B.; Lundstrom, T.; Christensen, H.; Jonsson, M.; de Pablo, J.; Rovira, M.; Clarens, F.; Casas, I.; Martinez-Esparza, A.; Gago, J.; Bruno, J.; Cera, E.; Merino, J.; Gonzalez de la Huebra, A.; Iglesias, E.; Quinones, J.; Cachoir, C.; Lemmens, K.; Mayer, G.; Jegou, C. *Spent fuel evolution under disposal conditions—Synthesis of results from the EU spent fuel stability (SFS) project*; Technical Report 04-09; Nagra: Wettingen, Switzerland, 2005.

(14) Poinssot, C.; Ferry, C.; Kelm, M.; Grambow, B.; Martinez-Esparza, A.; Johnson, L.; Adriambololona, Z.; Bruno, J.; Cachoir, C.; Cavedon, J. M.; Christensen, H.; Corbel, C.; Jegou, C.; Lemmens, K.; Loida, A.; Lovera, P.; Miserque, F., de Pablo, J.; Poulesquen, A.; Quinones, J.; Rondinella, V. V.; Spahiu, K.; Wegen, D. *Final Report of the European Project Spent Fuel stability under Repository Conditions*; Report CEA-R-6093; CEA: London, 2005.

(15) Cachoir, C.; Carbol, P.; Cobos-Sabate, J.; Glatz, J. P.; Lemmens, K.; Martínez-Esparza, A.; Mennecart, T.; Ronchi, C.; Rondinella, V. V.; Serrano-Purroy, D.; Spahiu, K.; Wegen, D. H.; Wiss, T. In *Effect of Alpha Irradiation Field on Long-Term Corrosion Rates of Spent Fuel, Spent fuel stability under repository conditions: SFS, Deliverable D9*; Grambow, B., Ed.; 2005; Contract FIKW-CT-2001-20192.

(16) Grambow, B.; Lemmens, K.; Minet, Y.; Poinssot, C.; Spahiu, K.; Bosbach, D.; Ignasi Casas, J.; de Pablo, J.; Giménez, J.; Gin, S.; Glatz, J. P.; Hyatt, N. C.; Iglesias, E.; Kienzler, B.; Luckscheiter, B.; Martinez-Esparza, A.; Metz, V.; Ödegaard-Jensen, A.; Ollila, K.; Quiñones, J.; Rey, A.; Ribet, S.; Rodriguez, N.; Skarnemark, G.; Wegen, D.; Rondinella, V. V.; Wiss, T.; Clarens, F.; Gonzalez-Robles, E.; Serrano-PurroyD. *Final Synthesis Report, RTD Component 1: Dissolution and release from the waste matrix, NF-PRO Deliverable*; NF-PRO Integrated Project; European Commission, DG-RTD; 2007; Contract FI6W-CT-2003-002389.

(17) Oversby, V. M. *Rates and mechanisms of radioactive release and retention inside a waste disposal canister (In Can Processes)*; Final Report European Commission, 2007; Contract FIKW-CT-2000-00019.

(18) Swift, P. N.; Knowles, K.; McNeish, J.; Hansen, C. W.; Howard, R. L.; MacKinnon, R.; Sevougian, S. D. *Mater. Res. Soc. Symp. Proc.* **2009**, *1124*, 3−14.

(19) Altmaier, M.; Kienzler, B.; Duro, L.; Grivé, M.; Montoya, V. *4th Annual Workshop Proceedings of the Collaborative Project "Redox Phenomena Controlling Systems" (7th EC FP CP RECOSY)*; KIT-SR 7626; Karlsruhe, Germany, 2012.

(20) FIRST-Nuclides, 2012, http://www.firstnuclides.eu/.

(21) Serrano-Purroy, D.; Casas, I.; González-Robles. E.; Glatz J. P.; Wegen, D. H.; Clarens, F.; Giménez, J.; de Pablo, J.; Martínez-Esparza, A. *J. Nucl. Mater.* **2012**, http://dx.doi.org/10.1016/j.jnucmat.2011.03.020.

(22) Serrano-Purroy, D.; Rondinella, V. V.; Wegen, D. H. *Characterisation of Irradiated MOX: Static leaching Report, NF-PRO Deliverable 1.4.10*; ITU Technical Report JRC-ITU-TPW-2007/37.

(23) González-Robles, E. Study of Radionuclide Release in commercials UO_2 Spent Nuclear Fuels. Doctoral Thesis, Universitat Politécnica de Catalunya, Barcelona, Spain, 2011.

(24) Rondinella, V. V.; Serrano-Purroy, D.; Hiernaut, J.-P.; Wegen, D.; Papaioannou, D.; Barker, M. Grain boundary inventory and instant release fractions for SBR MOX. *Proceedings of the International High-Level Radioactive Waste Management Conference*, Las Vegas, NV, Sept 7−9, 2008; Paper 195780 (ANS CD-ROM).
(25) ORIGEN-ARP 2000, Automatic Rapid Process for Spent Fuel depletion, Decay, and Source Term Analysis; NUREG/CR-0200, Revision 6; 2000; Vol. *l*, Section D1; ORNL/NUREG/CSD-2/V1/R6.
(26) de Pablo, J.; Serrano-Purroy, D.; Gonzalez-Robles, E.; Clarens, F.; Martínez-Esparza, A.; Wegen, D. H.; Casas, I.; Christiansen, B.; Glatz, J.-P.; Giménez, J. *Mater. Res. Soc. Symp. Proc.* **2009**, *1193*, 613−620.
(27) Fernandez, A. M. *Preparacion de una agua intersticial sintetica bentonitica a diferentes salinidades (Preparation of a synthetic bentonitic interstitial water at different salinities)*; 2005; CIEMAT DMA/M214213/05.
(28) Casas, I.; de Pablo, J.; Clarens, F.; Gimenez, J.; Merino, J.; Bruno, J.; Martinez-Esparza, A. *Radiochim. Acta* **2009**, *97*, 485−490.
(29) Rondinella, V. V.; Matzke, Hj.; Cobos, J.; Wiss, T. *Radiochim. Acta* **2000**, *88*, 527−531.
(30) Rondinella, V. V.; Cobos, J.; Wiss, T.; Hiernaut, J.-P. Studies on spent fuel alterations during storage and radiolysis effects on corrosion behaviour using alpha-doped UO_2. *Proceedings of ICEM '03*, Oxford, U.K., Sept 21−25, 2003; ASME: New York, 2003 (CD-ROM).
(31) Rondinella, V. V.; Cobos, J.; Wiss, T.; Staicu, D. Studies on spent fuel alterations during storage and effects on corrosion behaviour. *Proceedings of ICEM '05*, Glasgow, U.K., Sept 5−8, 2005; ASME: New York, 2005 (CD-ROM); Paper 1275.
(32) Rondinella, V. V.; Wiss, T.; Papaioannou, D.; Nasyrow, R. Studies on nuclear fuel evolution during storage and testing of used fuel response to impact loadings. *Proceedings of PSAM11-ESREL*, June 25−29, 2012, Helsinki, Finland, 2012; in press.
(33) Wiss, T.; Rondinella, V. V.; Cobos, J.; Wegen, D. H.; Amme, M.; Ronchi, C. Studies on Spent Fuel Corrosion Behaviour at JRC-ITU. *Proceedings of Atalante*, Nimes, France, June 21−25, 2004; CEA: London, 2004 (CD-ROM); Paper P3-34.
(34) Carbol, P.; Cobos-Sabaté, J.; Glatz, J.-P.; Ronchi, C.; Rondinella, V. V.; Wegen, D. H.; Wiss, T. *The effect of dissolved hydrogen on the dissolution of ^{233}U doped $UO_2(s)$, high burn-up spent fuel and MOX fuel*; Swedish Nuclear Fuel and Waste Management Co.: Stockholm, Sweden, 2005; SKB TR-05-09.
(35) Cobos, J.; Rondinella, V. V.; Matzke, Hj.; Martinez-Esparza, A.; Wiss, T. The effect of α-radiolysis on the dissolution behaviour of UO_2. *Proceedings of the International Conference on Future Nuclear Systems GLOBAL '99*, Jackson Hole, WY, Aug 29−Sept 3, 1999; American Nuclear Society: La Grange Park, IL, 1999 (CD-ROM).
(36) Cobos, J.; Serrano, J. A.; Glatz, J. P.; de Pablo, J.; Sätmark, B. The kinetic of dissolution of irradiated UO_2 fuel under oxidising conditions in flow experiments. *Proceedings of ICEM'01*, Bruges, Belgium, Sept 30−Oct 4, 2001 (CD-ROM).
(37) Cobos, J.; Havela, L.; Rondinella, V. V.; De Pablo, J.; Gouder, T.; Glatz, J. P.; Carbol, P.; Matzke, Hj. *Radiochim. Acta* **2002**, *90*, 597−602.
(38) Cobos, J.; Wiss, T.; Gouder, T.; Rondinella, V. V. *Mater. Res. Soc. Symp. Proc.* **2003**, *757*, 365−375.
(39) Fernandez, A.; Richter, K.; Fourcaudot, S.; Closset, J. C.; Fuchs, C.; Babelot, J. F.; Voet, R.; Somers, J. *Adv. Sci. Technol.* **1999**, *24*, 539−546.
(40) Somers, J.; Voet, R.; Fuchs, C.; Hein, H.; Boshoven, C.; Fourcaudot, S.; Modery, N.; Murray-Farthing, M. *Fabrication of UO_2 pellets doped with ^{233}U for α-radiolysis investigations*; Technical Report JRC-ITU-TPW-2001/12.
(41) Ziegler, J. F.; Biersack, J. P.; Littmark, U. *The Stopping and Range of Ions in Solids*; Pergamon Press: London, 1985.
(42) Miller, W.; Kline, A.; Hanson, B. Dosimetry modeling at the fuel−water interface. *Proceedings of the 11th International High-Level Radioactive Waste Management Conference (IHLRWMC)*, Las Vegas, NV, 2006; American Nuclear Society: La Grange Park, IL, 2006; pp 698−711.
(43) Solatie, D.; Carbol, P.; Betti, M.; Bocci, F.; Hiernaut, T.; Rondinella, V. V.; Cobos, J. *Fresenius' J. Anal. Chem.* **2000**, *368*, 88−94.
(44) Rondinella, V. V.; Betti, M.; Bocci, F.; Hiernaut, T.; Cobos, J. *Microchem. J.* **2001**, *67/1*−3, 305−308.
(45) Fors, P.; Carbol, P.; Van Winckel, S.; Spahiu, K. *J. Nucl. Mater.* **2009**, *394*, 1−8.
(46) Kleykamp, H. *J. Nucl. Mater.* **1985**, *131*, 463.
(47) Cui, D.; Rondinella, V. V.; Fortner, J. A.; Kropf, A. J.; Eriksson, L.; Wronkiewicz, D. J.; Spahiu, K. *J. Nucl. Mater.* **2012**, *420*, 328−333.
(48) Rondinella, V. V.; Wiss, T. *Mater. Today* **2010**, *13* (12), 24−32.
(49) Wiss, T. Radiation Effects in UO_2. In *Comprehensive Nuclear Materials*; Konings, R. J. M., Ed.; Elsevier: Amsterdam, The Netherlands, 2012; Vol. *5*, pp 465−480.
(50) Rondinella, V. V.; Wiss, T.; Hiernaut, J.-P.; Staicu, D. Dose Rate Effects on the Accumulation of Radiation Damage. *Proceedings of ICEM '07*, Bruges, Belgium, Sept 2−6, 2007; ASME: New York, 2007 (CD-ROM); Paper 7322.
(51) Rondinella, V. V.; Wiss, T.; Maugeri, E.; Colle, J.-Y. Effects of helium build-up on nuclear fuel evolution during storage. *Proceedings of IHLRWMC*, Albuquerque, NM, April 10−14, 2011; American Nuclear Society: La Grange Park, IL, 2011; pp 230−233; Paper 3458.
(52) Staicu, D.; Wiss, T.; Rondinella, V. V.; Hiernaut, J. P.; Konings, R. J. M.; Ronchi, C. *J. Nucl. Mater.* **2010**, *397*, 8−18.
(53) Maugeri, E.; Wiss, T.; Hiernaut, J.-P.; Desai, K.; Thiriet, C.; Rondinella, V. V.; Colle, J.-Y.; Konings, R. J. M. *J. Nucl. Mater.* **2009**, *385*, 461−466.
(54) Maugeri, E. Ph.D. Thesis, Universitá degli Studi di Pavia, Pavia, Italy, 2009.
(55) Ronchi, C.; Hiernaut, J.-P. *J. Nucl. Mater.* **2004**, *325*, 1−12.
(56) Ferry, C.; Poinssot, C.; Cappelaere, C.; Desgranges, L.; Jegou, C.; Miserque, F.; Piron, J. P.; Roudil, D.; Gras, J. M. *J. Nucl. Mater.* **2006**, *352* (1−3), 246−253.
(57) Ferry, C.; Piron, J.-P.; Ambard, A. *J. Nucl. Mater.* **2010**, *407*, 100−109.
(58) Ferry, C.; Piron, J.-P.; Stout, R. *Mater. Res. Soc. Symp. Proc.* **2007**, *985*, 65−70.
(59) Garisto, N. C.; Johnson, L. H.; Hocking, W. H. *Proceedings of the 2nd International CANDU Fuel Conference*, Chalk River, Ontario, Canada, Oct 1989; Chalk River Laboratories: Chalk River, Ontario, Canada, 1989; p 352.
(60) Stroes-Gascoyne, S.; Tait, J. C.; Garisto, N. C.; Porth, R. J.; Ross, J. P. M.; Glowa, G. A.; Barnsdale, T. R. *Mater. Res. Soc. Symp. Proc.* **1992**, *257*, 373−380.
(61) Johnson, L.; Ferry, C.; Poinssot, C.; Lovera, P. *Estimates of the Instant Release Fraction for UO_2 and MOX fuels at $t = 0$*; Nagra: Wettingten, Switzerland, 2004; TR 04-08.
(62) Johnson, L.; Ferry, C.; Poinssot, C.; Lovera, P. *J. Nucl. Mater.* **2005**, *346*, 56−65.
(63) Johnson, L.; Günther-Leopold, I.; Kobler Waldis, J.; Linder, H. P.; Low, J.; Cui, D.; Ekeroth, E.; Spahiu, K.; Evins, L. Z. *J. Nucl. Mater.* **2012**, *420*, 5−62.
(64) Gray, W. J.; Strachan, D. M. *Mater. Res. Soc. Symp. Proc.* **1991**, *212*, 205.
(65) Gray, W. J.; Thomas, L. E. *Mater. Res. Soc. Symp. Proc.* **1994**, *333*, 391.
(66) Gray, W. J. *Spent fuel dissolution rates as a function of burn-up and water chemistry*; 1998; Report PNL-11895.
(67) Gray, W. J. *Mater. Res. Soc. Symp. Proc.* **1999**, *556*, 487.
(68) Hanson, B.; Hanson, B. D.; Stout, R. B. *Mater. Res. Soc. Symp. Proc.* **2004**, *824*, 89−94.
(69) Roudil, D.; Jégou, C.; Broudic, V.; Muzeau, B.; Peuget, S.; Deschanels, X. *J. Nucl. Mater.* **2007**, *362*, 411.
(70) Roudil, D.; Jégou, C.; Broudic, V.; Tribet, M. *Mater. Res. Soc. Symp. Proc.* **2009**, *1193*, 627−633.
(71) Ferry, C.; Piron, J. P.; Poulesquen, A.; Poinssot, C. *Mater. Res. Soc. Symp. Proc.* **2008**, *1107*, 447−454.
(72) Martínez-Esparza, A.; Gago, J. A.; Quiñones, J.; Iglesias, E.; Pérez de Andrés, S. *Review of Influence of burn-up and irradiation history on spent fuel instant release, NF-PRO Deliverable 1.4.2*; NF-PRO

Integrated Project, European Commission, DG-RTD, 2003; Contract FI6W-CT-2003-002389.
(73) Jégou, C.; Caraballo, R.; De Bonfils, J.; Broudic, V.; Peuget, S.; Vercouter, T.; Roudil, D. *J. Nucl. Mater.* **2010**, *399*, 68−80.
(74) Poinssot, C.; Toulhoat, P.; Gras, J.-M.; Vitorge, P. *J. Nucl. Sci. Technol.* **2002**, No. suppl. 3, 473−476.
(75) Poinssot, C.; Lovera, P.; Faure, M.-H. *Mater. Res. Soc. Symp. Proc.* **2002**, *713*, JJ14.2.
(76) Forsyth, R. SKB Technical Report 95-23, 1995.
(77) Serrano, J. A.; Rondinella, V. V.; Glatz, J.-P.; Toscano, E. H.; Quiñones, J.; Diaz-Arocas, P. P.; Garcia-Serrano, J. *Radiochim. Acta* **1998**, *82*, 32−37.
(78) Poinssot, C.; Ferry, C.; Lovera, P.; Jegou, C.; Gras, J.-M. *J. Nucl. Mater.* **2005**, *346*, 66−77.
(79) Thomas, L. E.; Einziger, R. E.; Buchanan, H. C. *J. Nucl. Mater.* **1993**, *201*, 310.
(80) Cobos, J.; Papaioannou, D.; Spino, J.; Coquerelle, M. *J. Alloys Compd.* **1998**, *271*−*273*, 610−615.
(81) Shoesmith, D. W. *Used Fuel and Uranium dissolution studies - A review*; Nuclear Waste Management Organization (NWMO): Toronto, Ontario, Canada, 2007; NWMO-TR-2007-03.
(82) Hanson, B. Examining the Conservatisms in Dissolution Rates of Commercial Spent Nuclear Fuel. *Proceedings of the 12th International High-Level Radioactive Waste Management Conference (IHLRWM)*; Las Vegas, NV, Sept 7−11, 2008; American Nuclear Society, La Grange Park, IL, 2008.
(83) Casella, A.; Hanson, B.; Miller, W. Factors Affecting UO_2 Dissolution Under Geologic Disposal Conditions. *Proceedings of the 12th International High-Level Radioactive Waste Management Conference (IHLRWMC)*, Las Vegas, NV, Sept 7−11, 2008; American Nuclear Society, La Grange Park, IL, 2008.
(84) Eriksen, T. E.; Shoesmith, D. W.; Jonsson, M. *J. Nucl. Mater.* **2012**, *420*, 409−423.
(85) Hiernaut, J.-P.; Papaioannou, D.; Wiss, T.; Konings, R. J. M.; Rondinella, V. V. *J. Nucl. Mater.* **2008**, *372*, 215−225.
(86) Shoesmith, D. W. *J. Nucl. Mater.* **2000**, *282*, 1−31.
(87) Pastina, B.; LaVerne, J. A. *J. Phys. Chem. A* **2001**, *105* (40), 9316−9322.
(88) Gray, W. J. *Mater. Res. Soc. Symp. Proc.* **1987**, *84*, 141−151.
(89) Gray, W. J.; Wilson, C. N. *Spent fuel dissolution studies: FY 1991 to 1994*; 1995; Report PNL-10540.
(90) Weber, W. J.; Wald, J. W.; McVay, G. L. *J. Am. Ceram. Soc.* **1985**, *68* (9), C-253−255.
(91) Christensen, H. *Mater. Res. Soc. Symp. Proc.* **1991**, *212*, 213−220.
(92) Christensen, H.; Sunder, S. AECL-11479 COG-95-535, 1995.
(93) Sunder, S.; Shoesmith, D. W.; Christensen, H.; Miller, N. H. *J. Nucl. Mater.* **1992**, *190*, 79−86.
(94) Eriksen, T. E.; Eklund, U.-B.; Werme, L.; Bruno, J. *J. Nucl. Mater.* **1995**, *227*, 76−82.
(95) Eriksen, T. E. SKB Progress Report U-96-29, 1996.
(96) Jégou, C.; Broudic, V.; Poulesquen, A.; Bart, J. M. *Mater. Res. Soc. Symp. Proc.* **2004**, *807*, 391−396.
(97) Loida, A.; Grambow, B.; Geckeis, H.; Dressler, P. *Mater. Res. Soc. Symp. Proc.* **1995**, *353*, 577−584.
(98) Loida, A.; Grambow, B.; Geckeis, H. *J. Nucl. Mater.* **1996**, *238*, 11.
(99) Röllin, S.; Spahiu, K.; Eklund, U. B. *J. Nucl. Mater.* **2001**, *297*, 231.
(100) Cera, E.; Bruno, J.; Duro, L.; Eriksen, T. *Experimental determination and chemical modelling of radiolytic processes at the spent fuel/water interface. Long contact time experiments*; Swedish Nuclear Fuel and Waste Management Co.: Stockholm, Sweden, 2006; SKB TR-06-07.
(101) Christensen, H.; Bjergbakke, E. *Mater. Res. Soc. Symp. Proc.* **1985**, *50*, 401−408.
(102) Shoesmith, D. W.; Sunder, S.; Johnson, L. H.; Bailey, M. G. *Mater. Res. Soc. Symp. Proc.* **1985**, *50*, 309−316.
(103) Sunder, S.; Shoesmith, D. W.; Johnson, L. H.; Wallace, G. J.; Bailey, M. G.; Snaglewski, A. P. *Mater. Res. Soc. Symp. Proc.* **1987**, *84*, 309−316.
(104) Sunder, S.; Shoesmith, D. W.; Christensen, H.; Bailey, M. G.; Miller, N. H. *Mater. Res. Soc. Symp. Proc.* **1989**, *127*, 317−324.
(105) Sunder, S.; Shoesmith, D. W.; Christensen, H.; Miller, N. H.; Bailey, M. G. *Mater. Res. Soc. Symp. Proc.* **1990**, *176*, 457−464.
(106) Sunder, S.; Shoesmith, D. W.; Miller, N. H. *J. Nucl. Mater.* **1997**, *244*, 66−74.
(107) Giménez, J.; Baraj, E.; Torrero, M. E.; Casas, I.; de Pablo, J. *J. Nucl. Mater.* **1996**, *238*, 64−69.
(108) Shoesmith, D. W.; Sunder, S. *J. Nucl. Mater.* **1992**, *190*, 20−35.
(109) Sattonnay, G.; Ardois, C.; Corbel, C.; Lucchini, J. F.; Barthe, M. F.; Garrido, F.; Gosset, D. *J. Nucl. Mater.* **2001**, *288*, 11.
(110) Stroes-Gascoyne, S.; King, F.; Betteridge, J. S.; Garisto, F. *Radiochim. Acta* **2002**, *90*, 603−609.
(111) Stroes-Gascoyne, S.; Betteridge, J. S. The effects of alpha-radiolysis on UO_2 dissolution determined from batch experiments with ^{238}Pu-doped UO_2. Presented at the MRS 2004 Symposium on the Scientific Basis for Nuclear Waste Management, San Francisco, 2004.
(112) Cachoir, C.; Lemmens, K. *Mater. Res. Soc. Symp. Proc.* **2004**, *807*, 59−64.
(113) Kelm, M.; Bohnert, E. Radiolytic Corrosion of ^{238}Pu-doped UO_2 Pellets in 5 M NaCl Solution. *Proceedings of the 2004 MRS Spring Meeting*; Volume *824*.
(114) Kelm, M.; Bohnert., E. *J. Nucl. Mater.* **2005**, *346*, 1−4.
(115) Ollila, K.; Albinsson, Y.; Oversby, V.; Cowper, M. SKB Report TR-03-13, 2003.
(116) Rondinella, V. V.; Cobos, J.; Matzke, Hj.; Wiss, T.; Carbol, P.; Solatie, D. *Mater. Res. Soc. Symp. Proc.* **2001**, *663*, 391−398.
(117) Marx G. In *Source term for performance assessment of spent fuel as a waste form*; Grambow, B. , et al., Ed.; EUR 19140, Luxembourg, 2000.
(118) Shoesmith, D. W.; Sunder, S.; Bailey, M. G.; Wallace, G. J. *Can. J. Chem.* **1988**, *66*, 259.
(119) Engelhardt, J.; Marx, G. *J. Nucl. Chem.* **1999**, *264*, 161.
(120) Stern, M.; Geary, A. L. *J. Electrochem. Soc.* **1957**, *104*, 56−63.
(121) Stern, M.; Method, A. *Corrosion* **1958**, *14*, 440t−444t.
(122) Wegen, D. H.; Bottomley, P. D. W.; Glatz, J.-P. The electrochemical modelling of irradiated UO_2 surface reactions in groundwater solution. *Proceedings of ICEM'01*, Bruges, Belgium, Sep 30−Oct 4, 2001.
(123) Lemmens, K. *Proceedings of the Spent Fuel Workshop*, Lake Forest, CA, Apr 19−20, 2004; American Nuclear Society, La Grange Park, IL, 2004.
(124) Ekeroth, E.; Jonsson, M. *J. Nucl. Mater.* **2003**, *322*, 242−248.
(125) Rosborg, B.; Werme, L. *J. Nucl. Mater.* **2008**, *379* (1−3), 142−153.
(126) Cui, D.; Ekeroth, E.; Fors, P.; Spahiu, K. *Mater. Res. Soc. Symp. Proc.* **2008**, *1104*, 1104-NN03-05.
(127) Garrels, R. M.; Christ, C. L. *Solutions, Minerals, and Equilibria*; Harper & Row: New York, 1965.
(128) Bonin, B.; Colin, M.; Dutfoy, A. *J. Nucl. Mater.* **2000**, *281* (1), 1−14.
(129) Liu, L.; Neretnieks., I. *Nucl. Technol.* **2002**, *138*, 69−77.
(130) Selin, P. P. SR 97: Hydromechanical evolution in a defective canister. *Scientific Basis for Nuclear Waste Management XXVI*; Material Research Society Symposium Series 663; Material Research Society: Warrendale, PA, 2001; pp 755−763.
(131) SERCO 2011. *Review of colloids in the geosphere and their treatment in performance assessment*; SERCO TAS Report 002924/01 issue 3; SERCO Harwell Science and Innovation Campus, Didcot, England, 2011.
(132) SKB 2006. *Long-term safety for KBS-3 repositories at Forsmark and Laxemar—a first evaluation Main Report of the SR-Can project*; SKB Technical Report TR-06-09; 2006.
(133) Cui, D.; Spahiu, K. *Radiochim. Acta* **2002**, *90*, 623−628.
(134) Scott, T. B.; Allen, G. C.; Heard, P. J.; Randell, M. G. *Geochim. Cosmochim. Acta* **2005**, *69* (24), 5639−5646.

(135) Loida, A.; Metz, V.; Kienzler, B.; Geckeis, H. *J. Nucl. Mater.* **2005**, *346*, 24−31.
(136) Metz, V.; Geckeis, H.; González-Robles, E.; Loida, A.; Bube, C.; Kienzler, B. *Radiochim. Acta* **2012**, DOI: 10.1524/ract.2012.1967.
(137) Spahiu, K.; Eklund, U.-B.; Cui, D.; Lundström, M. *Mater. Res. Soc. Symp. Proc.* **2002**, *713*, 633−638.
(138) Spahiu, K.; Devoy, J.; Cui, D.; Lundström, M. *Radiochim. Acta* **2004**, *92*, 597−601.
(139) Loida, A.; Grambow, B.; Geckeis, H. Spent Fuel Corrosion Behavior in Salt Solution in the Presence of Hydrogen Overpressure. *Proceedings of ICEM'01*, Bruges, Belgium, Sept 30−Oct 4, 2001; pp 711−716 (CD-ROM).
(140) Carbol, P.; Fors, P.; Van Winckel, S.; Spahiu, K. *J. Nucl. Mater.* **2009**, *392*, 45−54.
(141) Spahiu, K.; Werme, L.; Eklund, U. B. *Radiochim. Acta* **2000**, *88*, 507.
(142) Neck, V.; Altmaier, M.; Fanghänel, Th. *C. R. Chim.* **2007**, *10*, 959−977.
(143) Carbol, P.; Fors, P.; Gouder, T.; Spahiu, K. *Geochim. Cosmochim. Acta* **2009**, *73*, 4366−4375.
(144) Jonsson, M.; Nielsen, F.; Roth, O.; Ekeroth, E.; Nilsson, S.; Hossain, M. M. *Environ. Sci. Technol.* **2007**, *41*, 7087−7093.
(145) Forsyth, R. S.; Werme, L. O.; Bruno, J. *J. Nucl. Mater.* **1986**, *138*, 1−15.
(146) Jégou, C.; Muzeau, B.; Broudic, V.; Roudil, D.; Deschanels, X. *Radiochim. Acta* **2007**, *95*, 513−522.